

1 **Evidence for adaptive evolution in the receptor-binding domain of**
2 **seasonal coronaviruses OC43 and 229E**

4 Kathryn E. Kistler^{1,2}, Trevor Bedford^{1,2}

6 ¹*Vaccine and Infectious Disease Division, Fred Hutchinson Cancer Research Center, Seattle,*
7 *WA USA*

8 ²*Molecular and Cellular Biology Program, University of Washington, Seattle, WA USA*

9 * To whom correspondence should be addressed.

10 **Abstract**

12 Seasonal coronaviruses (OC43, 229E, NL63 and HKU1) are endemic to the human population,
13 regularly infecting and reinfecting humans while typically causing asymptomatic to mild
14 respiratory infections. It is not known to what extent reinfection by these viruses is due to
15 waning immune memory or antigenic drift of the viruses. Here, we address the influence of
16 antigenic drift on immune evasion of seasonal coronaviruses. We provide evidence that at least
17 two of these viruses, OC43 and 229E, are undergoing adaptive evolution in regions of the viral
18 spike protein that are exposed to human humoral immunity. This suggests that reinfection may
19 be due, in part, to positively-selected genetic changes in these viruses that enable them to
20 escape recognition by the immune system. It is possible that, as with seasonal influenza, these
21 adaptive changes in antigenic regions of the virus would necessitate continual reformulation of a
22 vaccine made against them.

23 **Introduction**

25 Coronaviruses were first identified in the 1960s and, in the decades that followed, human
26 coronaviruses (HCoVs) received a considerable amount of attention in the field of infectious
27 disease research. At this time, two species of HCoV, OC43 and 229E, were identified as the
28 causative agents of roughly 15% of common colds (McIntosh 1974; Heikkinen and Järvinen
29 2003). Infections with these viruses were shown to exhibit seasonal patterns, peaking in
30 January-March in the Northern Hemisphere, as well as yearly variation, with the greatest
31 incidence occurring every 2-4 years (Monto and Lim 1974; Hamre and Beem 1972).

32 Subsequently, two additional seasonal HCoVs, HKU1 and NL63, have entered the human
33 population. These 4 HCoVs endemic to the human population usually cause mild respiratory
34 infections, but occasionally result in more severe disease in immunocompromised patients or
35 the elderly (D. X. Liu, Liang, and Fung 2020). In the past 20 years, three additional HCoVs
36 (SARS-CoV-1, MERS-CoV and SARS-CoV-2) have emerged, which cause more severe
37 respiratory illness. At the writing of this paper, amidst the SARS-CoV-2 pandemic, no vaccine
38 for any HCoV is currently available, though many candidate SARS-CoV-2 vaccines are in
39 production and clinical trials (Krammer 2020).

41 Coronaviruses are named for the ray-like projections of spike protein that decorate their surface.
42 Inside these virions is a positive-sense RNA genome of roughly 30kB (F. Li 2016). This large
43 genome size can accommodate more genetic variation than a smaller genome (Woo et al.

44 2009). Genome flexibility, coupled with a RNA virus error-prone polymerase (Drake 1993) and a
45 high rate of homologous recombination (Pasternak, Spaan, and Snijder 2006), creates genetic
46 diversity that is acted upon by evolutionary pressures that select for viral replication. This
47 spawns much of the diversity within and between coronaviruses species (Woo et al. 2009; Hon
48 et al. 2008), and can contribute to the virus' ability to jump species-barriers, allowing a
49 previously zoonotic CoV to infect and replicate in humans.

50
51 The battle between virus and host results in selective pressure for mutations that alter viral
52 antigens in a way that evades immune recognition. Antigenic evolution, or antigenic drift, leaves
53 a characteristic mark of positively selected epitopes within the viral proteins most exposed to the
54 host immune system (Smith et al. 2004). For CoVs, this is the spike protein, exposed on the
55 surface of the virion to human humoral immunity. Some human respiratory illnesses caused by
56 RNA viruses, like seasonal influenza (Smith et al. 2004), evolve antigenically, while others, like
57 measles, do not (Fulton et al. 2015a). Because of this, seasonal influenza vaccines must be
58 reformulated on a nearly annual basis, while measles vaccines typically provide lifelong
59 protection. Whether HCoVs undergo antigenic drift is relevant not only to understanding HCoV
60 evolution and natural immunity against HCoVs, but also to predicting the duration of a vaccine's
61 effectiveness.

62
63 Early evidence that closely-related HCoVs are antigenically diverse comes from a 1980s human
64 challenge study in which subjects were infected and then reinfected with a variety of 229E-
65 related strains (Reed 1984). All subjects developed symptoms and shed virus upon initial virus
66 inoculation. After about a year, subjects who were re-inoculated with the same strain did not
67 show symptoms or shed virus. However, the majority of subjects who were re-inoculated with a
68 heterologous strain developed symptoms and shed virus. This suggests that immunity mounted
69 against 229E viruses provides protection against some, but not all, other 229E strains. This is a
70 result that would be expected of an antigenically evolving virus.

71
72 More recent studies have identified 8 OC43 genotypes and, in East Asian populations, certain
73 genotypes were shown to temporally replace other genotypes (Lau et al. 2011; Y. Zhang et al.
74 2015; Zhu et al. 2018). Whether certain genotypes predominate due to antigenic differences
75 that confer a fitness advantage is not known. However, evidence for selection in the spike
76 protein of one of these dominant OC43 genotypes has been provided by *dN/dS*, a standard
77 computational method for detecting positive selection (Ren et al. 2015). This method has also
78 been used to suggest positive selection in the spike protein of 229E (Chibo and Birch 2006).
79 Additionally, two genetically distinct groupings (each of which include multiple of the
80 aforementioned 8 genotypes) of OC43 viruses have been shown to alternate in prevalence
81 within a Japanese community, meaning that the majority of OC43 infections are caused by one
82 group for about 2-4 years at which point the other group begins to account for the bulk of
83 infections. It has been suggested that antigenic differences between these groups contribute to
84 this epidemic switching (Komabayashi et al. 2020).

85
86 However, a similar surveillance of the NL63 genotypes circulating in Kilifi, Kenya found that
87 NL63 genotypes persist for relatively long periods of time, that people become reinfected by the

88 same genotype, and that reinfections are often enhanced by prior infection (Kiyuka et al. 2018).
89 These findings are inconsistent with antigenic evolution in NL63.

90
91 Here, we use a variety of computational approaches to detect adaptive evolution in spike and
92 comparator proteins in HCoVs. These methods were designed as improvements to dN/dS with
93 the intention of identifying adaptive substitutions within a serially-sampled RNA virus population.
94 We focus on the seasonal HCoVs that have been continually circulating in humans: OC43,
95 229E, HKU1 and NL63. Our analyses of nonsynonymous divergence, rate of adaptive
96 substitutions, and Time to Most Recent Ancestor (TMRCA) provide evidence that the spike
97 protein of OC43 and 229E is under positive selection. Though we conduct these analyses on
98 HKU1 and NL63, we do not observe evidence for adaptive evolution in the spike protein of
99 these viruses. For HKU1, there is not enough longitudinal sequencing data available for us to
100 confidently make conclusions as to whether or not this lack of evidence reflects an actual lack of
101 adaptive evolution.

102

103 **Results**

104 *Phylogenetic consideration of viral diversity and recombination in OC43 and 229E*

105 We constructed time-resolved phylogenies of the OC43 and 229E using publicly accessible
106 sequenced isolates. A cursory look at these trees confirms previous reports that substantial
107 diversity exists within each viral species (Y. Zhang et al. 2015; Komabayashi et al. 2020; Lau et
108 al. 2011). Additionally, the trees form ladder-like topologies with isolate tips arranged into
109 temporal clusters rather than geographic clusters, indicating a single global population rather
110 than geographically-isolated populations of virus. The phylogeny of OC43 bifurcates
111 immediately from the root (Figure 1), indicating that OC43 consists of multiple, co-evolving
112 lineages. Because of the distinct evolutionary histories, it is appropriate to conduct phylogenetic
113 analyses separately for each lineage. We have arbitrarily labeled these lineages 'A' and 'B'
114 (Figure 1).

115

116 Because recombination is common amongst coronaviruses (Pasternak, Spaan, and Snijder
117 2006; Hon et al. 2008; Lau et al. 2011), we built separate phylogenies for each viral gene. In the
118 absence of recombination, each tree should show the same evolutionary relationships between
119 viral isolates. A dramatic difference in a given isolate's position on one tree versus another is
120 strongly indicative of recombination (Kosakovsky Pond et al. 2006). Comparing the RNA-
121 dependent RNA polymerase (RdRp) and spike trees reveals this pattern of recombination in
122 some isolates (Figure 1- figure supplement 1A). A comparison of the trees of the S1 and S2
123 sub-domains of spike shows more limited evidence for intragenic recombination (Figure 1-figure
124 supplement 1B), which is consistent with the fact that the distance between two genetic loci is
125 inversely-related to the chance that these loci remain linked during a recombination event.
126 Though intragenic recombination likely does occur occasionally, analyzing genes, rather than
127 isolates, greatly reduces the contribution of recombination to genetic variation in our analyses.

128

129 Thus, in all of our analyses, we use alignments and phylogenies of sequences of single genes
130 (or genomic regions) rather than whole genome sequences of isolates. We designate the
131 lineage of those genes (or genomic regions) based on the gene's phylogeny. Though most

132 isolates contain all genes from the same lineage, some isolates have, say, a lineage A spike
133 gene and a lineage B RdRp gene. This strategy allows us to consider the evolution of each
134 gene separately, and interrogate the selective pressures acting on them.

135
136 It is worth noting that the analyses we use here to detect adaptive evolution canonically
137 presume that selective pressures are acting on single nucleotide polymorphisms (SNPs).
138 However, it is possible that recombination also contributes to the genetic variation that is acted
139 on by immune selection. This would be most likely to occur if two closely-related genomes
140 recombine, resulting in the introduction of a small amount of genetic diversity without disrupting
141 crucial functions. Our analyses do not aim to determine the source of genetic variation (i.e.
142 SNPs or recombination), but rather focus on identifying if and how selection acts on this
143 variation.

144
145 Because of its essential role in viral replication and lack of antibody exposure, we expect RdRp
146 to be under purifying selection to maintain its structure and function. If HCoVs evolve
147 antigenically, we expect to see adaptive evolution in spike, and particularly in the S1 domain of
148 spike (Hofmann et al. 2006; Hulswit et al. 2019), due to its exposed location at the virion's
149 surface and interaction with the host receptor. Mutations that escape from population immunity
150 are beneficial to the virus and so are driven to fixation by positive selection. This results in
151 adaptive evolution of the virus population.

152
153 *Phylogenetic inference of substitution prevalence within spike*
154 Using phylogenies constructed from the spike gene, we tallied the number of independent
155 amino acid substitutions at each position within spike. The average number of substitutions per
156 site is higher in S1 than S2 for HCoV lineages in OC43 and 229E (Figure 2A). We focus on S1
157 rather than the Receptor-Binding Domain (RBD) within S1 in our analyses, because it is known
158 that neutralizing antibodies bind to epitopes within the N-Terminal Domain (NTD) as well as the
159 RBD of S1 (L. Liu et al. 2020; S. Zhang et al. 2018; Zhou et al. 2019). A greater occurrence of
160 repeated substitutions is expected if some mutations within S1 confer immune avoidance.
161 Alternatively, these repeated substitutions could be a result of high mutation rate and random
162 genetic drift as has been shown at particular types of sites in SARS-CoV-2 (van Dorp et al.
163 2020). However, this latter hypothesis should affect all regions of the genome equally and
164 should not result in a greater number of repeated substitutions in S1 than S2.

165
166 If the repeated mutations are a product of immune selection, not only should S1 contain more
167 repeated mutations, but we would also expect these mutations to spread widely after they occur
168 due to their selective advantage. Additionally, we expect sites within S1 to experience
169 diversifying selection due to the ongoing arms race between virus and host immune system.
170 This is visible in the distribution of genotypes at the most repeatedly-mutated sites in OC43
171 lineage A (Figure 2B and 2C).

172
173 *Nonsynonymous and synonymous divergence in RdRp and subdomains of spike*
174 An adaptively evolving gene, or region of the genome, should exhibit a high rate of
175 nonsynonymous substitutions. For each seasonal HCoV lineage, we calculated nonsynonymous

176 and synonymous divergence as the average Hamming distance from that lineage's most recent
177 common ancestor (Zanini et al. 2015). The rate of nonsynonymous divergence is markedly
178 higher within spike versus RdRp of 229E and OC43 lineage A (Figure 3A). While
179 nonsynonymous divergence increases steadily over time in spike, it remains roughly constant at
180 0.0 in RdRp. These results suggest that there is predominantly positive selection on OC43 and
181 229E spike, but predominantly purifying selection on RdRp. Separating spike into the S1
182 (receptor-binding) and S2 (membrane-fusion) domains reveals that the majority of
183 nonsynonymous divergence in spike occurs within S1 (Figure 3B). In fact, the rates of
184 nonsynonymous divergence in S2 are similar to those seen in RdRp, suggesting S2 evolves
185 under purifying selection while S1 evolves adaptively.

186

187 Though we would expect synonymous divergence to be equivalent in all areas of the genome,
188 this is not born out in our results. It is unclear whether the difference in synonymous divergence
189 between genes reflects an actual biological difference. However, the ratio of nonsynonymous
190 divergence in spike to nonsynonymous divergence in RdRp is consistently higher than the
191 equivalent ratio of synonymous divergence (Figure 3- figure supplement 2). Thus, despite
192 differences in synonymous divergence, spike is accumulating more relatively more
193 nonsynonymous divergence than RdRp.

194

195 We compared our analysis of divergence to the results a more standard approach for detecting
196 positive selection on certain branches of a phylogeny. This approach, called MEME, is
197 maximum-likelihood method which gives a single dN/dS value for each gene (Murrell et al.
198 2012; Weaver et al. 2018). In agreement with measures of nonsynonymous divergence over
199 time, dN/dS estimates are higher in Spike than RdRp and higher in S1 than S2 (Table 2). Our
200 estimate of dN/dS in OC43 spike is similar to the previously reported estimate of roughly 0.3
201 (Ren et al. 2015). However, we believe the standard dN/dS approach is not the ideal tool for
202 detecting adaptive evolution in HCoVs because it is a phylogenetic approach, which may be
203 biased by recombination, and also because some assumptions of the model hold true for
204 mammalian genomes, but not necessarily for RNA viruses.

205

	RdRp	Spike	S1	S2
229E	0.143	0.441	0.662	0.166
OC43 lineage A	0.080	0.435	0.466	0.301
OC43 lineage B	0.061	0.317	0.418	0.234
NL63	0.068	0.139	0.121	0.038

206 **Table 1. dN/dS is lower in Spike than RdRp.** A single dN/dS value was computed for gene (or spike
207 domain) and each HCoV using MEME.

208

209 *Rate of Adaptation in RdRp and subdomains of spike*
210 Therefore, as a complement to the divergence analysis, we implemented an alternative to the
211 *dN/dS* method that was specifically designed to detect positive selection within RNA virus
212 populations (Bhatt, Holmes, and Pybus 2011). Compared with traditional *dN/dS* methods, the
213 Bhatt method has the advantages of: 1) measuring the strength of positive selection within a
214 population given sequences collected over time, 2) higher sensitivity to identifying mutations
215 that occur only once and sweep through the population, and 3) correcting for deleterious
216 mutations (Bhatt, Katzourakis, and Pybus 2010; Bhatt, Holmes, and Pybus 2011). Briefly, this
217 method defines a class of neutrally-evolving nucleotide sites as those with synonymous
218 mutations or where nonsynonymous polymorphisms occur at medium frequency. Then, the
219 number of fixed and high-frequency nonsynonymous sites that exceed the neutral expectation
220 are calculated. This method compares nucleotide sequences at each timepoint (the ingroup) to
221 the consensus nucleotide sequence at the first time point (the outgroup) and yields an estimate
222 of the number of adaptive substitutions within a given genomic region at each of these
223 timepoints.
224
225 We adapted this method to detect adaptive substitutions in seasonal HCoVs. As shown in
226 Figure 4, OC43 lineage A has continuously amassed adaptive substitutions in spike over the
227 past >30 years while RdRp has accrued few, if any, adaptive substitutions. These adaptive
228 substitutions are located within the S1, and not the S2, domain of spike (Figure 4). We observe
229 a largely linear accumulation of adaptive substitutions in spike and S1 through time, although
230 the method does not dictate a linear increase. This observation suggests that spike (and S1 in
231 particular) is evolving in response to a continuous selective pressure. This is exactly what would
232 be expected if these adaptive substitutions are evidence of antigenic evolution resulting from an
233 evolutionary arms race between spike and the host immune system.
234
235 We estimate that OC43 lineage A accumulates roughly 0.61×10^{-3} adaptive substitutions per
236 codon per year (or 0.45 adaptive amino acid substitutions in S1 each year) in the S1 domain of
237 spike, while the rate of adaptation in OC43 lineage B is slightly higher and is estimated to result
238 in an average 0.56 adaptive substitutions in S1 per year (Figure 5). The S1 domain of 229E is
239 estimated to accrue 0.26 adaptive substitutions per year (a rate of 0.47×10^{-3} adaptive
240 substitutions per codon per year).
241
242 A benefit of the Bhatt method is the ability to calculate the strength of selection, which allows us
243 to compare these seasonal HCoVs to other viruses. We used our implementation of the Bhatt
244 method to calculate the rate of adaptation for influenza A/H3N2, which is known to undergo
245 rapid antigenic evolution (Rambaut et al. 2008; Yang 2000), measles, which does not (Fulton et
246 al. 2015a), and influenza B strains Vic and Yam, which evolve antigenically at a slower rate than
247 A/H3N2 (Bedford et al. 2014). We estimate that the receptor-binding domain of influenza
248 A/H3N2 accumulates adaptive substitutions between 2 and 3 times faster than the HCoVs
249 OC43 and 229E (Figure 6). The rate of adaptive substitution in influenza B/Yam and B/Vic are
250 on par with the seasonal HCoVs. We detect no adaptive substitutions in the measles receptor-
251 binding protein. These results put the evolution of the S1 domain of OC43 and 229E in context,
252 indicating that the S1 domain is under positive selection, and that this positive selection

253 generates new variants in the putative antigenic regions of these HCoVs at about the same rate
254 as influenza B strains and about half the rate of the canonical example of antigenic evolution,
255 the HA1 domain of influenza A/H3N2.

256

257 *Validation that rate of adaptation is not biased by recombination*

258 Because coronaviruses are known to recombine, and recombination has the potential to impact
259 evolutionary analyses of selection, we sought to verify that our results are not swayed by the
260 presence of recombination. To do this, we simulated the evolution of OC43 lineage A spike and
261 RdRp genes under varying levels of recombination and positive selection (representative
262 phylogenies of simulated spike evolution can be seen in Figure 7- figure supplement 2) and
263 used our implementation of the Bhatt method to identify adaptive evolution. As the strength of
264 positive selection increases, we detect a higher rate of adaptive evolution, regardless of the
265 level of recombination (Figure 7). This demonstrates that our estimates of adaptive evolution are
266 not biased by recombination events.

267

268 *Time to Most Recent Common Ancestor (TMRCA) of RdRp and subdomains of spike*

269 Finally, we know that strong directional selection skews the shape of phylogenies (Volz, Koelle,
270 and Bedford 2013). In influenza H3N2, immune selection causes the genealogy to adopt a
271 ladder-like shape where the rungs are formed by viral diversification and each step is created by
272 the appearance of new, antigenically-superior variants that replace previous variants. This
273 ladder-like shape can also be seen in the phylogenies of the OC43 and 229E (Figure 1). In this
274 case, selection can be quantified by the timescale of population turnover as measured by the
275 Time to Most Recent Common Ancestor (TMRCA), with the expectation that stronger selection
276 will result in more frequent steps and therefore a smaller TMRCA measure (Bedford, Cobey,
277 and Pascual 2011). We computed average TMRCA values from phylogenies built on Spike, S1,
278 S2 or RdRp sequences of OC43 lineage A and 229E (Table 2). We did not compute TMRCA for
279 OC43 lineage B because the limited number of available RdRp sequences for this lineage mean
280 that TMRCA can only be calculated for about 4 years, which could artificially skew the TMRCA
281 estimates. Our estimates of HCoV spike TMRCA are roughly 2-2.5 longer the estimated
282 TMRCA for influenza A/H3N2 hemagglutinin (Bedford, Cobey, and Pascual 2011).

283

284 We observe that, for both OC43 lineage A and 229E, the average TMRCA is lower in spike than
285 RdRp and lower in S1 versus S2. These results suggest strong directional selection in S1, likely
286 driven by pressures to evade the humoral immune system. The difference in TMRCA between
287 S1 and S2 is indicative not only of differing selective pressures acting on these two spike
288 domains, but also of intra-spike recombination. This is because the immune selection imposed
289 on S1, should also propagate neutral hitch-hiker mutations in closely-linked regions such as S2.
290 The difference in TMRCA suggests that recombination may uncouple these regions.

291 Recombination can also push TMRCA to higher values, though this should not have a larger
292 impact on RdRp than S1. The contributions of the forces of directional selection and
293 recombination are difficult to parse from the TMRCA results. This emphasizes the importance of
294 using methods, such as the Bhatt method, that are robust to recombination to detect adaptive
295 evolution.

296

	Spike	S1	S2	RdRp
OC43 lineage A	4.67 (4.04, 5.28)	3.45 (2.86, 4.05)	13.05 (11.24, 14.97)	17.39 (15.63, 19.15)
229E	4.19 (3.13, 5.25)	2.23 (1.76, 2.69)	5.08 (3.93, 6.23)	4.86 (4.04, 5.69)

297 **Table 2. Mean TMRCA is lower in S1 than RdRp or S2.** Average TMRCA values (in years) for OC43
 298 lineage A and 229E. The 95% confidence intervals are indicated in parentheses below mean TMRCA
 299 values.

300

301 *Application of methods for identifying adaptive evolution to HKU1 and NL63*

302 Because HKU1 was identified in the early 2000's, there are fewer longitudinally-sequenced
 303 isolates available for this HCoV compared to 229E and OC43 (Figure 1- figure supplement 2).
 304 Consequently, the phylogenetic reconstructions and divergence analysis of HKU1 have a higher
 305 level of uncertainty. To begin with, it is less clear from the phylogenies whether HKU1
 306 represents a single HCoV lineage like 229E or, instead, should be split into multiple lineages
 307 like OC43 (Figure 1). Because of this, we completed all antigenic analyses for HKU1 twice:
 308 once considering all isolates to be members of a single lineage, and again after splitting isolates
 309 into 2 separate lineages. These lineages are arbitrarily labeled 'A' and 'B' as was done for
 310 OC43. When HKU1 is considered to consist of just one lineage, there is no signal of antigenic
 311 evolution by divergence analysis (Figure 3- figure supplement 1B) or by the Bhatt method of
 312 estimating adaptive evolution (Figure 5- figure supplement 1A). However, when HKU1 is
 313 assumed to consist of 2 co-circulating lineages, HKU1 lineage A has a markedly higher rate of
 314 adaptive substitutions in S1 than in S2 or RdRp (Figure 5- figure supplement 1B).

315

316 To demonstrate the importance of having a well-sampled longitudinal series of sequenced
 317 isolates for our antigenic analyses, we returned to our simulated OC43 S1 datasets. We
 318 mimicked shorter longitudinal series by truncating the dataset to only 24, 14, 10, or 7 years of
 319 samples and ran the Bhatt analysis on these sequentially shorter time series (Figure 7- figure
 320 supplement 1). The rates of adaptation estimated from the truncated datasets can be compared
 321 to the "true" rate of adaptation calculated from all simulated data. This simulated data reveals a
 322 general trend that less longitudinal data reduces the ability to detect adaptive evolution by
 323 skewing the estimated rate away from the "truth" and increasing the uncertainty of the analysis.
 324 Given the dearth of longitudinal data for HKU1, we do not feel that it is appropriate to make
 325 strong conclusions about adaptive evolution, or lack thereof, in this HCoV.

326

327 Despite being identified at roughly the same time as HKU1, substantially more NL63 isolates
 328 have been sequenced (Figure 1- figure supplement 2) making the phylogenetic reconstruction
 329 and evolutionary analyses of this virus correspondingly more reliable. We do not observe
 330 evidence for adaptive evolution in NL63 (Figure 3- figure supplement 1A and Figure 5- figure
 331 supplement 1A) and this lack of support for adaptive evolution in the NL63 spike gene is more
 332 likely to reflect an actual lack of adaptive evolution in this virus.

333

334 **Discussion**

335 Using several corroborating methods, we provide evidence that the seasonal HCoVs OC43 and
336 229E undergo adaptive evolution in S1, the region of the spike protein exposed to human
337 humoral immunity (Figures 3, 4 and 5). We additionally confirm that RdRp and S2 do not show
338 signals of adaptive evolution. We observe that S1 accumulates between 0.3 (229E) and 0.5
339 (OC43) adaptive substitutions per year. We infer that these viruses accumulate adaptive
340 substitutions at roughly half the rate of influenza A/H3N2 and at a similar rate to influenza B
341 viruses (Figure 6). The most parsimonious explanation for the observation of substantial
342 adaptive evolution in S1 is that antigenic drift is occurring in which mutations that escape from
343 human population immunity are selectively favored in the viral population leading to repeated
344 adaptive changes. However, it is formally possible that the adaptive evolution we detect is a
345 result of selective pressures other than evasion of the adaptive immune system. Showing that
346 this is truly antigenic evolution could involve a serological comparison of isolates that differ at S1
347 residues under positive selection.

348

349 In seasonal influenza and measles, the rates of adaptive evolution we estimate correlate well
350 with relative rates of antigenic drift reported by other groups (Fulton et al. 2015b; Bedford et al.
351 2014). The relative rates of adaptation we calculate also match the relative frequency of vaccine
352 strain updates, as would be expected since vaccines must be updated to match antigenically-
353 evolving viruses. Since 2006, the A/H3N2 component of the seasonal influenza vaccine has
354 been updated 10 times (11 different A/H3N2 strains), 4 different B/Vic strains and 4 different
355 B/Yam strains have been included in the vaccine, and the measles vaccine strain has not
356 changed (Global Influenza Surveillance and Response System
357 (GISRS), <https://www.who.int/influenza/vaccines/virus/en/>). Using these numbers as guidance,
358 our results suggest that a vaccine against OC43 or 229E might need to be updated as
359 frequently as the B/Vic and B/Yam components of the influenza vaccine are.

360

361 We do not observe evidence of antigenic evolution in NL63 (Figure 3-figure supplement 1 and
362 Figure 5- figure supplement 1). This likely represents a lack of marked adaptive evolution in S1.
363 Our finding fits with a study of NL63 in Kenya, which identified multiple genotypes of NL63 and
364 show that people regularly become reinfected with the same genotype of NL63 (Kiyuka et al.
365 2018). Additionally, Kiyuka et al found that these genotypes circulate locally for a long period of
366 time, suggesting a decent amount of viral diversity and a potential lack of evolution due to
367 immune selection. Though our results cannot explain why OC43 and 229E likely evolve
368 antigenically while NL63 does not, Kiyuka et al observe that NL63 reinfections are sometimes
369 enhanced by a previous infection and hypothesize that NL63 is actually under purifying
370 selection at epitope sites (Kiyuka et al. 2018).

371

372 Though analysis of all HCoVs would benefit from more sequenced isolates, there is
373 substantially less longitudinal sequencing data available for HKU1. Thus, despite finding no
374 evidence of antigenic evolution in HKU1 (Figure 3-figure supplement 1 and Figure 5- figure
375 supplement 1), it is possible that a more completely sampled time series of HKU1 genome
376 sequences could alter the result for this virus (Figure 7-figure supplement 1).

377

378 Our conclusions of adaptive evolution in S1, arrived at through computational analyses of
379 sequencing data, agree with studies that observe reinfection of subjects by heterologous
380 isolates of 229E (Reed 1984), sequential dominance of specific genotypes of OC43 (Lau et al.
381 2011; Y. Zhang et al. 2015), and common reinfection by seasonal HCoVs from longitudinal
382 serological data (Edridge et al. 2020). In this latter study, HCoV infections were identified from
383 longitudinal serum samples by assaying for increases in antibodies against the nucleocapsid (N)
384 protein of representative OC43, 229E, HKU1, and NL63 viruses. This study concluded that the
385 average time between infections was 1.5–2.5 years, depending on the HCoV (Edridge et al.
386 2020). In comparison, influenza H3N2 reinfects people roughly every 5 years (Kucharski et al.
387 2015). Thus, frequent reinfection by seasonal HCoVs is likely due to a combination of factors
388 and suggests waning immune memory, and/or incomplete immunity against reinfection, in
389 addition to antigenic drift.

390
391 Human coronaviruses are a diverse grouping split, phylogenetically, into two genera: NL63 and
392 229E are alphacoronaviruses, while OC43, HKU1, MERS, SARS, and SARS-CoV-2 are
393 betacoronaviruses. The method of cell-entry does not seem to correlate with genus.
394 Coronaviruses bind to a remarkable range of host-cell receptors including peptidases, cell
395 adhesion molecules and sugars. Amongst the seasonal HCoVs, OC43 and HKU1 both bind 9-
396 O-acetylsialic acid (Hulswit et al. 2019), while 229E binds human aminopeptidase N (hAPN) and
397 NL63 binds angiotensin-converting enzyme 2 (ACE2) (D. X. Liu, Liang, and Fung 2020).
398 Despite a relatively large phylogenetic distance and divergent S1 structures, NL63 and SARS-
399 CoV-1 and SARS-CoV-2 bind to the same host receptor using the same virus-binding motifs
400 (VBMs) (F. Li 2016). This VBM is located in the C-terminal domain of S1 (S1-CTD), which fits
401 within the trend of S1-CTD receptor-binding in CoVs that bind protein receptors (Hofmann et al.
402 2006; F. Li 2016). This is opposed to the trend amongst CoVs that bind sugar receptors, where
403 receptor-binding is located within the S1 N-terminal domain (S1-NTD) (F. Li 2016). This
404 localization roughly aligns with our observations that the majority of the repeatedly-mutated sites
405 occur toward the C-terminal end of 229E S1 and the N-terminal end of OC43 S1 (Figure 2).
406

407 Here, we have provided support that at least 2 of the 4 seasonal HCoVs evolve adaptively in the
408 region of spike that is known to interact with the humoral immune system. These two viruses
409 span both genera of HCoVs, though due to the complexity of HCoV receptor-binding and
410 pathology mentioned above, it is not clear whether or not this suggests that other HCoVs, such
411 as SARS-CoV-2, will also evolve adaptively in S1. This is important because, at the time of
412 writing of this manuscript, many SARS-CoV-2 vaccines are in production and most of these
413 exclusively include spike (Krammer 2020). If SARS-CoV-2 evolves adaptively in S1 as the
414 closely-related HCoV OC43 does, it is possible that the SARS-CoV-2 vaccine would need to be
415 frequently reformulated to match the circulating strains, as is done for seasonal influenza
416 vaccines.
417

418 Materials and methods

419 All data, source code and analyses can be found at [https://github.com/blab/seasonal-cov-
420 adaptive-evolution](https://github.com/blab/seasonal-cov-adaptive-evolution). All phylogenetic trees constructed and analyzed in this manuscript can be
421 viewed interactively at <https://nextstrain.org/community/blab/seasonal-cov-adaptive-evolution>.

422 All analysis code is written in Python 3 (Python Programming Language, SCR_008394) in
423 Jupyter notebooks (Jupyter-console, RRID:SRC_018414).
424

425 **Sequence data**

426 All viral sequences are publicly accessible and were downloaded from ViPR (www.viprbrc.org)
427 under the “Coronaviridae” with host “human” (Pickett et al. 2012). Sequences labeled as
428 “OC43”, “229E”, “HKU1” and “NL63” were pulled out of the downloaded FASTA file into 4
429 separate data files. Additionally, a phylogeny of all downloaded human coronaviruses was made
430 and unlabeled isolates that clustered within clades formed by labeled OC43, 229E, HKU1 or
431 NL63 isolates were marked as belonging to that HCoV type and added to our data files. Code
432 for these data-parsing steps is located in `data-`
433 `wrangling/postdownload_formatting_for_rerun.ipynb`.
434

435 **Phylogenetic inference**

436 For each of the 4 HCoV datasets, full-length sequences were aligned to a reference genome
437 using the augur align command (Hadfield et al. 2018) and MAFFT (Katoh et al. 2002). Individual
438 gene sequences were then extracted from these alignments if sequencing covered 50% or more
439 of the gene using the code in `data-`
440 `wrangling/postdownload_formatting_for_rerun.ipynb`. Sequence files for each
441 gene are located in the `data/` directory within each HCoV parent directory (ex:
442 `oc43/data/oc43_spike.fasta`). A Snakemake file (Köster and Rahmann 2012) within each
443 HCoV directory follows the general outline of a Nextstrain build (Nextstrain, RRID:SCR_018223)
444 and was used to align each gene to a reference strain and build a time-resolved phylogeny with
445 IQ-Tree v1 (Nguyen et al. 2015) and TimeTree (Sagulenko, Puller, and Neher 2018).
446 Phylogenies were viewed to identify the distribution of genotypes throughout the tree, different
447 lineages, and signals of recombination using the nextstrain view command (Hadfield et al.
448 2018). The clock rate of the phylogeny based on spike sequences for each isolate (as shown in
449 Fig. 1 and Fig. 1 Supplement 2) was 0.0005 substitutions per nucleotide site per year for OC43,
450 0.0006 for 229E, 0.0007 for NL63, and 0.0062 for HKU1. All NL63 and HKU1 trees were rooted
451 on an outgroup sequence. For NL63, the outgroup was
452 `229e/AF304460/229e_ref/Germany/2000` and for HKU1 the outgroup was
453 `mhv/NC_048217_1/mhv/2006`. Clock rates for the phylogenies built on each individual gene can
454 be found within the `results/` directory within each HCoV parent directory (ex:
455 `oc43/results/branch_lengths_oc43_spike.json`).
456

457 **Mutation counting**

458 Amino acid substitutions at each position in spike were tallied from the phylogeny. In other
459 words, the phylogenetic reconstruction of spike sequences returns nucleotides changes to the
460 ancestral sequence along each branch. The number of times this changed amino acid identity at
461 each position was tallied. This analysis was conducted using code in
462 `antigenic_evolution/site_mutation_rank.ipynb`.
463

464 **Divergence analysis**

465 For each HCoV lineage and each gene, synonymous and nonsynonymous divergence was
466 calculated at all timepoints as the average Hamming distance between each sequenced isolate
467 and the consensus sequence at the first timepoint (founder sequence). The total number of
468 observed differences between the isolate and founder nucleotide sequences that result in
469 nonsynonymous (or synonymous) substitutions is divided by the number of possible nucleotide
470 mutations that result in nonsynonymous (or synonymous) substitutions, weighted by kappa, to
471 yield an estimate of divergence. Kappa is the ratio of rates of transitions:transversions, and was
472 calculated by averaging values from spike and RdRp trees built by BEAST 2.6.3 (Bouckaert et
473 al. 2019) using the HKY+gamma4 model with 2 partitions and “coalescent constant population”.
474 All BEAST results are found in .log files in gene- and HCoV-specific subdirectories within
475 beast/. Divergence is calculated from nucleotide alignments. Sliding 3-year windows were
476 used and only timepoints that contained at least 2 sequences were considered. The concept for
477 this analysis is from (Zanini et al. 2015) and code for our adaptation is in
478 antigenic_evolution/divergence_weighted.ipynb. The ratios of divergence shown in
479 Figure 3- figure supplement 2 are also calculated in this notebook.
480

481 ***Calculation of dN/dS***

482 A dN/dS value was calculated for RdRp, spike, S1 and S2 of each HCoV using the Datammonkey
483 (Weaver et al. 2018) implementation of MEME (Mixed Effects Model of Evolution) (Murrell et al.
484 2012). Aligned FASTA files (ex: oc43/results/aligned_oc43_rdrp.fasta) were
485 uploaded to Datammonkey (<http://datammonkey.org/meme>) and dN/dS value was recorded as the
486 calculated Global MG94xREV model non-synonymous/synonymous rate ratio.
487

488 ***Implementation of the Bhatt method***

489 The rate of adaptive evolution was computed using an adaptation of the Bhatt method (Bhatt,
490 Holmes, and Pybus 2011; Bhatt, Katzourakis, and Pybus 2010). For each lineage and each
491 genomic region, we partitioned all available sequences into sliding 3-year windows and only
492 used timepoints that contained at least 3 sequences in the analysis. We compared nucleotide
493 sequences at each timepoint (the ingroup) to the consensus nucleotide sequence at the first
494 time point (the outgroup). Eight estimators (silent fixed, replacement fixed, silent high frequency,
495 replacement high frequency, silent mid-frequency, replacement mid-frequency, silent low
496 frequency and replacement low-frequency) are calculated by the site-counting method (Bhatt,
497 Katzourakis, and Pybus 2010). In the site-counting method, each estimator is the product of the
498 fixation or polymorphism score times the silent or replacement score, summed for each site in
499 that frequency class. Fixation and polymorphism scores depend on the number of different
500 nucleotides observed at the site and whether the outgroup base is present in the ingroup.
501 Selectively neutral sites are assumed to contain the classes of silent polymorphisms and
502 replacement polymorphisms occurring at a frequency between 0.15 and 0.75. A class of
503 nonneutral, adaptive sites is then identified as having an excess of replacement fixations or
504 polymorphisms (Bhatt, Holmes, and Pybus 2011). For each lineage and gene, 100 bootstrap
505 alignments and ancestral sequences were generated and run through the Bhatt method to
506 assess the statistical uncertainty of our estimates of rates of adaptation (Bhatt, Holmes, and
507 Pybus 2011). The rate of adaptation (per codon per year) shown in Fig. 5 is calculated by linear
508 regression of the time series values of adaptive substitutions per codon (Fig. 4). Our code for

509 implementing the Bhatt method is at
510 `antigenic_evolution/bhatt_bootstrapping.ipynb`.
511
512 ***Estimation of rates of adaptation of measles and influenza viruses***
513 Influenza and measles alignments were generated by running Nextstrain the respective
514 Nextstrain builds from <https://github.com/nextstrain/seasonal-flu> and
515 [https://github.com/nextstrain/measles_\(Hadfield et al. 2018\)](https://github.com/nextstrain/measles_(Hadfield et al. 2018)). The seasonal influenza build was
516 run with 20 year resolution for H3N2, H1N1pdm, Vic and Yam. The rates of adaptation of
517 different genes was calculated using our implementation of the Bhatt method described above.
518 The receptor-binding domain used for influenza was HA1, for measles was the H protein, and
519 for the HCoVs was S1. The membrane fusion protein used for influenza was HA2, for measles
520 was the F protein, and for the HCoVs was S2. The polymerase for influenza was PB1, for
521 measles was the P protein, and for the HCoVs was RbRd (nsp12). Our code for this analysis is
522 at `antigenic_evolution/bhatt_nextstrain.ipynb`.
523

524 ***Simulation of evolving OC43 sequences***
525 The evolution of OC43 lineage A Spike and RdRp genes was simulated using SANTA-SIM
526 (Jariani et al. 2019). The OC43 lineage A root sequence was used as a starting point and the
527 simulation was run for 500 generations and 10 simulated sequences were sampled every 50
528 generations. The spike and RdRp genes were simulated separately. Purifying selection was
529 simulated across both genes. Evolution was simulated in the absence of recombination and with
530 moderate and high levels of recombination during replication. Under each of these
531 recombination paradigms, we simulated evolution in the absence of positive selection within
532 spike and with moderate and high levels of positive selection. Positive selection was simulated
533 through exposure-dependent selection at a subset of spike S1 sites proportional to the number
534 of epitope sites in H3N2 HA (Luksza and Lässig 2014). The simulated selection allows
535 mutations in these “epitope” sites to rise in frequency while also encouraging “epitopes” to
536 change over time (to mimic antigenic novelty). All simulations were run with a nucleotide
537 mutation rate of 1x10-4 (Vijgen et al. 2005). Config files, results and source code for these
538 simulations can be at `santa-sim_oc43a/` and the Bhatt method is implemented on the
539 simulated data in `antigenic_evolution/bhatt_simulated_oc43_data.ipynb`.
540

541 ***Estimation of TMRCA***
542 Mean TMRCA values were estimated for each gene and each HCoV using PACT (Bedford,
543 Cobey, and Pascual 2011). Briefly, PACT computes TMRCA values by creating a series of
544 subtrees that include only tips positioned within a temporal slice of the full tree and finding the
545 common ancestor of these tips. The overall mean and 95% confidence interval were calculated
546 from the list of TMRCA values in these time slices. The PACT config files and results for each
547 run are in the directory `antigenic_evolution/pact/`. The TMRCA estimations and
548 subsequent analyses are executed by code in `antigenic_evolution/tmrca_pact.ipynb`.
549

550 **Acknowledgments**

551 We thank Jesse Bloom and members of the Bedford lab for useful feedback. KEK was
552 supported by the National Science Foundation Graduate Research Fellowship Program under

553 Grant No. DGE-1762114. TB is a Pew Biomedical Scholar and is supported by NIH R35
554 GM119774-01.

555

556 Competing Interests

557 The authors declare no competing interests.

558

559

560

561

562

563

564

565

566

567

568

569

570

571

572

573

574

575

576

577

578

579

580

581

582

583

584

585 Figure Legends

586

587 **Figure 1. Phylogenetic trees for spike gene of seasonal HCoVs OC43 and 229E.** Phylogenies built
588 from A: OC43 spike sequences from 389 isolates over 53 years, and B: 229E spike sequences from 54
589 isolates over 31 years. OC43 bifurcates immediately after the root and is split into two lineages: lineage A
590 (dark teal) and lineage B (light teal). 229E contains just one lineage (dark blue). For the analyses in
591 this paper, the evolution of each gene (or genomic region) is considered separately, so phylogenies are
592 built for each viral gene, and those phylogenies are used to split isolates into lineages for each gene.
593 These are temporally resolved phylogenies with year shown on the x-axis. The clock rate estimate is $5 \times$
594 10^{-4} substitutions per nucleotide site per year for OC43 and 6×10^{-4} for 229E.

595

596 **Figure 2. More sites mutate repeatedly within spike S1 versus S2.** A: Number of substitutions
597 observed at each amino acid position in the spike gene throughout the phylogeny. S1 (gray) and S2

598 (white) are indicated by shading and the number of substitutions per site is indicated by a dot and color-coded by HCoV lineage. The putative receptor-binding domains for 229E (Z. Li et al. 2019) and the
599 putative domain for OC43 (Lau et al. 2011) are indicated with light yellow bars. Asterisks indicate two
600 example positions (192 and 262), which mutate repeatedly throughout the OC43 lineage A phylogeny.
601 The OC43 phylogeny built from spike sequences and color-coded by genotype at position 192 and 262 is
602 shown in B) and C), respectively.

604

605 **Figure 3. Nonsynonymous divergence is higher in OC43 and 229E Spike S1 versus S2 or RdRp.** A:
606 Nonsynonymous (dashed lines) and synonymous divergence (solid lines) of the spike (dark orange) and
607 RdRp (dark gray) genes of all 229E and OC43 lineages over time. Divergence is the average Hamming
608 distance from the ancestral sequence, computed in sliding 3-year windows which contain at least 2
609 sequenced isolates. Shaded region shows 95% confidence intervals. Note that the absence of a line
610 means there fewer than 2 sequences available at this timepoint and that, therefore, the divergence is not
611 calculated. B: Nonsynonymous and synonymous divergence within the S1 (light orange) and S2 (light
612 gray) domains of spike. Year is shown on the x-axis and is shared between plots.

613

614 **Figure 4. Adaptive substitutions accumulate over time in OC43 lineage A spike S1.** Adaptive
615 substitutions per codon within OC43 lineage A spike, S1, S2 and RdRp as calculated by our
616 implementation of the Bhatt method. Adaptive substitutions are computed in sliding 3-year windows, and
617 only for timepoints that contain 3 or more sequenced isolates. Red dots display estimated values
618 calculated from the empirical data and red lines show linear regression fit to these points. Grey lines show
619 the distribution of regressions fit to the computed number of adaptive substitutions from 100 bootstrapped
620 datasets. Year is shown on the x-axis.

621

622 **Figure 5. The rate of adaptive substitution is highest in spike S1.** Adaptive substitutions per codon
623 per year as calculated by our implementation of the Bhatt method. Rates are calculated within Spike, S1,
624 S2 and RdRp for 229E and OC43 lineages. Error bars show 95% bootstrap percentiles from 100
625 bootstrapped datasets.

626

627 **Figure 6. OC43 and 229E spike S1 accumulates adaptive substitutions faster than measles but**
628 **slower than influenza A/H3N2.** Comparison of adaptive substitutions per codon per year between
629 measles (yellow), 4 influenza strains (A/H3N2, A/H1N1pdm, B/Vic and B/Yam- shown in shades of red),
630 OC43 lineage A (dark teal), OC43 lineage B (light teal), and 229E (dark blue). The polymerase, receptor
631 binding domain and membrane fusion domain for influenza strains are PB1, HA1 and HA2. For both
632 HCoVs, they are RdRp, S1 and S2, respectively. For measles, the polymerase is the P gene, the
633 receptor-binding protein is the H gene and the fusion protein is the F gene. Error bars show 95%
634 bootstrap percentiles from 100 bootstrapped datasets.

635

636 **Figure 7. Detection of positive selection is not biased by recombination.** OC43 lineage A sequences
637 were simulated with varying levels of recombination and positive selection. The Bhatt method was used to
638 calculate the rate of adaptive substitutions per codon per year for S1 (light orange), S2 (light gray) and
639 RdRp (dark gray). The mean and 95% confidence interval of 10 independent simulations is plotted.

640

641 **Figure 1- figure supplement 1. Recombination occurs between HCoV isolates.** A tanglegram draws
642 lines between an isolate's position on two phylogenies built on different genes (or genomic regions).
643 Dramatic differences in an isolate's position on one tree versus another is indicative of recombination. A)
644 Phylogenetic relationships between OC43 isolates based on spike sequences (left) versus relationships
645 based on RdRp sequences (right). Light teal lines that connect isolates classified as lineage A based on

646 their RdRp sequence to isolates classified as lineage B based on their spike sequence suggest that
647 recombination occurred in these isolates or their ancestors. B) Phylogenetic reconstruction of OC43
648 isolates based on S1 sequences (left) versus S2 sequences (right). Year is shown on the x-axis.
649

650 **Figure 1- figure supplement 2. Phylogenetic trees for seasonal HCoVs NL63 and HKU1.**

651 Phylogenies built from A: NL63 spike sequences from 159 isolates over 37 years, and B: HKU1 spike
652 sequences from 41 isolates over 13 years. HKU1 bifurcate immediately after the root and is split into
653 lineage A (darker blue) and lineage B (lighter blue). NL63 contains just one lineage (green). Both HCoVs
654 are rooted on an outgroup sequence. For the analyses in this paper, the evolution of each gene (or
655 genomic region) is considered separately, so phylogenies are built for each viral gene and those
656 phylogenies are used to split isolates into lineages for each gene. These are temporally resolved
657 phylogenies with year shown on the x-axis. The clock rate of each HCoV is listed in the Methods
658 "Phylogenetic inference" section.
659

660 **Figure 2- figure supplement 1. Mutations per at each position within Spike for NL63 and HKU1.**

661 Number of substitutions observed at each amino acid position in the spike gene throughout the phylogeny
662 S1 (gray) and S2 (white) are indicated by shading and the number of substitutions per site is indicated by
663 a dot and color-coded by HCoV lineage.. A: NL63, B: HKU1 (assuming all HKU1 isolates are a single
664 lineage), C: HKU1 lineage A, D: HKU1 lineage B (assuming there are 2 co-circulating HKU1 lineages).
665

666 **Figure 3- figure supplement 1. Nonsynonymous divergence in NL63 and HKU1.** Nonsynonymous
667 (dashed lines) and synonymous divergence (solid lines) within the spike (dark orange) and RdRp (dark
668 gray) genes and within S1 (light orange) and S2 (light gray) over time. Divergence is the average
669 Hamming distance from the ancestral sequence, computed in sliding 3-year windows which contain at
670 least 2 sequenced isolates. Shaded region shows 95% confidence intervals. A: NL63, B: HKU1
671 (assuming all HKU1 isolates belong to a single lineage), and C: HKU1 (divided into 2 co-circulating
672 lineages). Year is shown on the x-axis. Note that x- and y-axis scales are shared between the subplots
673 but are different than Figure 3.
674

675 **Figure 3- figure supplement 2. Ratio of divergence between genomic regions.** A: the ratio of
676 nonsynonymous divergence in spike to nonsynonymous divergence in RdRp (dashed lines) and the
677 equivalent ratio of synonymous divergence (solid lines) is shown for 229E (dark blue), OC43 lineage A
678 (dark teal), and OC43 lineage B (light teal). B: the same ratios of divergence as in panel A, except
679 comparing S1 and S2. Year is on the x-axis.
680

681 **Figure 5- figure supplement 1. NL63 and HKU1 have low rates of adaptation in spike.** As in Figure 4,
682 adaptive substitutions per codon per year are calculated by our implementation of the Bhatt method. A:
683 NL63 (green) and HKU1 (blue) are both considered to consist of a single lineage. B: HKU1 is divided into
684 2 co-circulating lineages (blue and light blue). The calculated rates of adaptive substitution within spike,
685 S1, S2 and RdRp are plotted alongside 229E and OC43 for comparison. Error bars show 95% bootstrap
686 percentiles from 100 bootstrapped datasets
687

688 **Figure 7- figure supplement 1. Fewer years of longitudinally-sampled isolates reduces ability to**
689 **detect rate of adaptation.** OC43 lineage A S1 sequences were simulated under conditions of no,
690 moderate and high rates of recombination in combination with no, moderate or high strength of positive
691 selection. The Bhatt method was used to calculate the "true" rate of adaptive evolution under each of
692 these scenarios using all available simulated sequence data (30 years), or the estimated rate if only the

693 most recent 24, 14, 10 or 7 years of simulated sequences were used. The mean and 95% confidence
694 intervals of 10 independent simulations are plotted.
695

696 **Figure 7- figure supplement 2. Representative phylogenies of simulated spike data.** OC43 lineage A
697 spike sequence evolution was simulated under conditions of no, moderate and high rates of
698 recombination in combination with no, moderate or high strength of positive selection. This figure shows
699 time-resolved phylogenies built from 1 of the 10 independent simulations under each
700 recombination/selection regime.

701

702 References

703

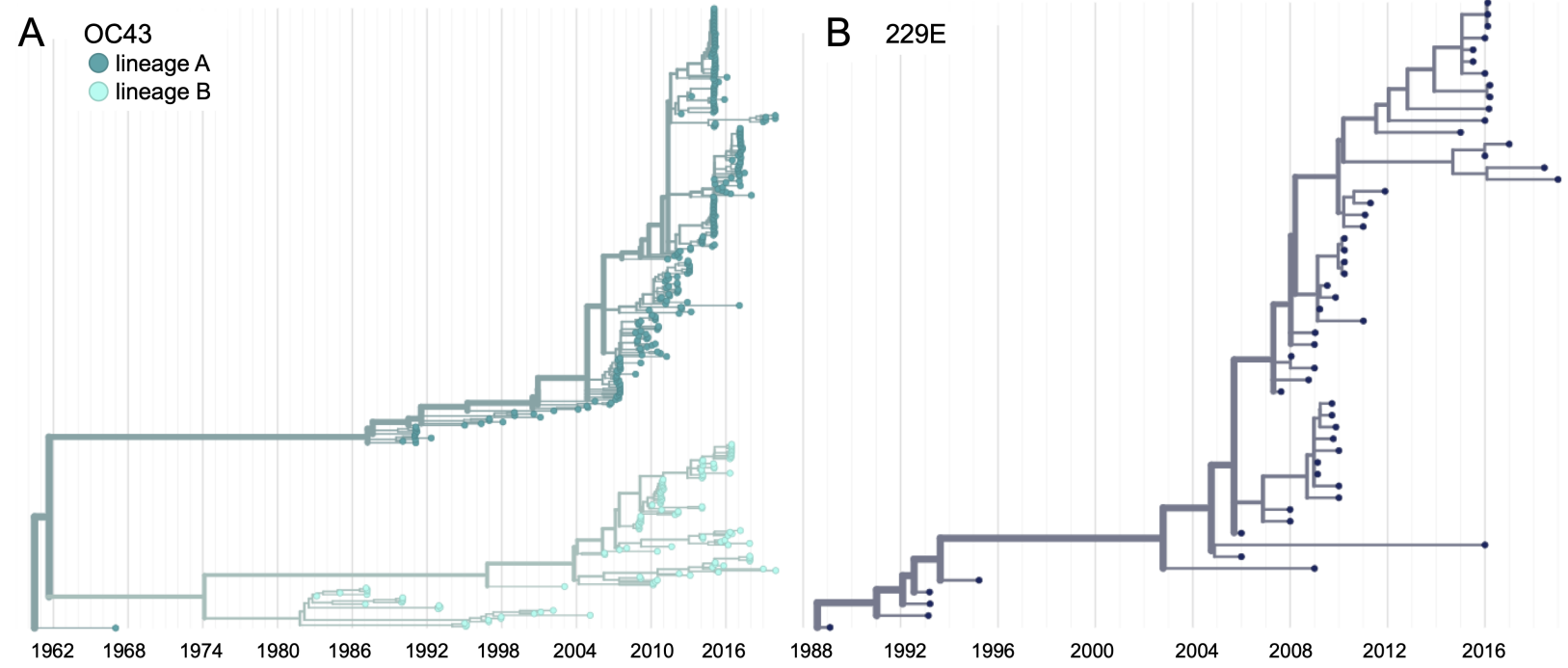
704

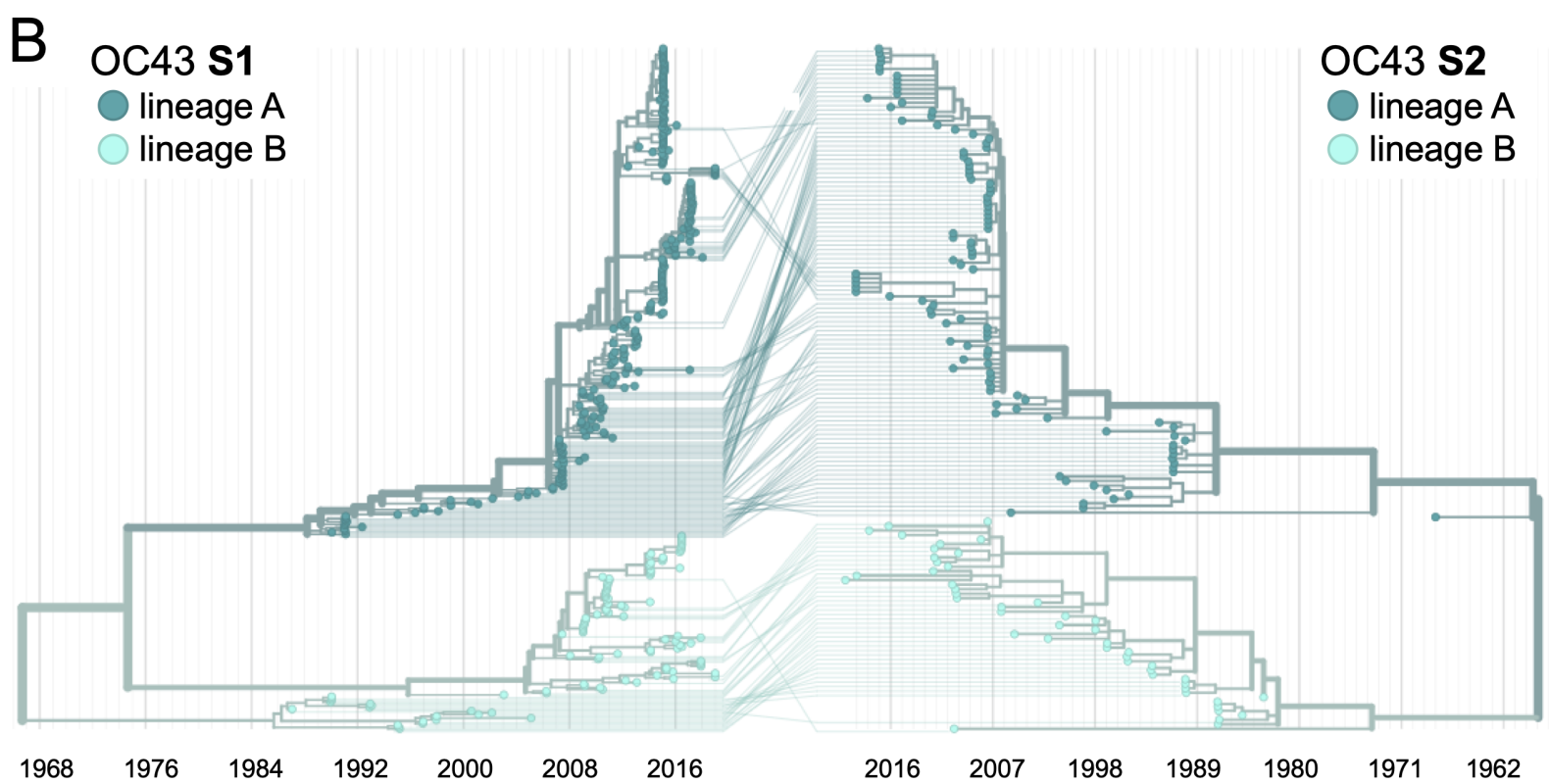
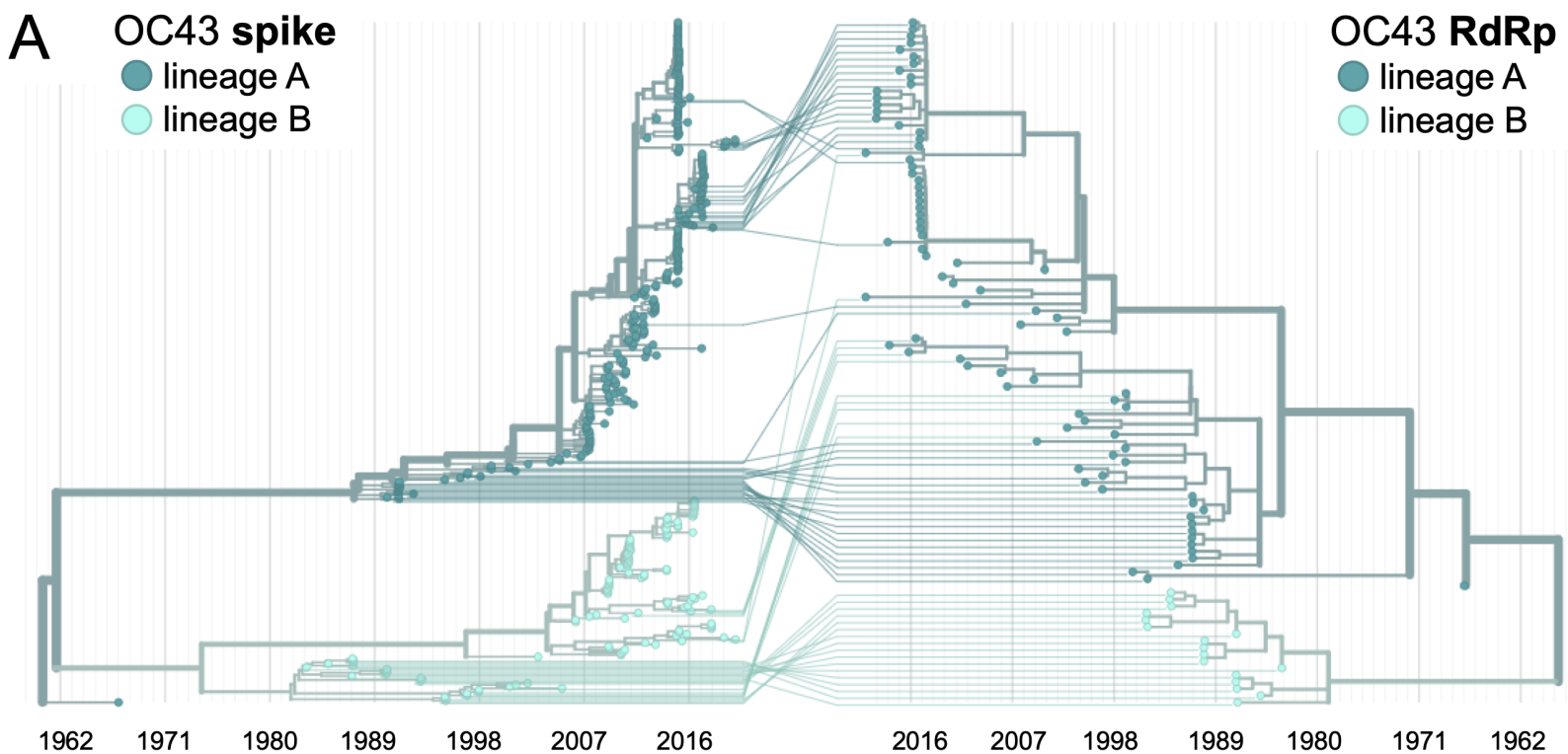
- 705 Bedford, Trevor, Sarah Cobey, and Mercedes Pascual. 2011. "Strength and Tempo of Selection
706 Revealed in Viral Gene Genealogies."
- 707 Bedford, Trevor, Marc A. Suchard, Philippe Lemey, Gytis Dudas, Victoria Gregory, Alan J. Hay,
708 John W. McCauley, Colin A. Russell, Derek J. Smith, and Andrew Rambaut. 2014.
709 "Integrating Influenza Antigenic Dynamics with Molecular Evolution." *ELife* 3 (February):
710 e01914.
- 711 Bhatt, Samir, Edward C. Holmes, and Oliver G. Pybus. 2011. "The Genomic Rate of Molecular
712 Adaptation of the Human Influenza A Virus." *Molecular Biology and Evolution* 28 (9):
713 2443–51.
- 714 Bhatt, Samir, Aris Katzourakis, and Oliver G. Pybus. 2010. "Detecting Natural Selection in RNA
715 Virus Populations Using Sequence Summary Statistics." *Infection, Genetics and
716 Evolution: Journal of Molecular Epidemiology and Evolutionary Genetics in Infectious
717 Diseases* 10 (3): 421–30.
- 718 Bouckaert, Remco, Timothy G. Vaughan, Joëlle Barido-Sottani, Sebastián Duchêne, Mathieu
719 Fourment, Alexandra Gavryushkina, Joseph Heled, et al. 2019. "BEAST 2.5: An
720 Advanced Software Platform for Bayesian Evolutionary Analysis." *PLoS Computational
721 Biology* 15 (4): e1006650.
- 722 Chibo, Doris, and Chris Birch. 2006. "Analysis of Human Coronavirus 229E Spike and
723 Nucleoprotein Genes Demonstrates Genetic Drift between Chronologically Distinct
724 Strains." *The Journal of General Virology* 87 (Pt 5): 1203–8.
- 725 Dorp, Lucy van, Damien Richard, Cedric C. S. Tan, Liam P. Shaw, Mislav Acman, and François
726 Balloux. 2020. "No Evidence for Increased Transmissibility from Recurrent Mutations in
727 SARS-CoV-2." *Nature Communications* 11 (1): 5986.
- 728 Drake, J. W. 1993. "Rates of Spontaneous Mutation among RNA Viruses." *Proceedings of the
729 National Academy of Sciences of the United States of America* 90 (9): 4171–75.
- 730 Edridge, Arthur W. D., Joanna Kaczorowska, Alexis C. R. Hoste, Margreet Bakker, Michelle
731 Klein, Katherine Loens, Maarten F. Jebbink, et al. 2020. "Seasonal Coronavirus
732 Protective Immunity Is Short-Lasting." *Nature Medicine*, September.
733 <https://doi.org/10.1038/s41591-020-1083-1>.
- 734 Fulton, Benjamin O., David Sachs, Shannon M. Beaty, Sohui T. Won, Benhur Lee, Peter
735 Palese, and Nicholas S. Heaton. 2015a. "Mutational Analysis of Measles Virus Suggests
736 Constraints on Antigenic Variation of the Glycoproteins." *Cell Reports* 11 (9): 1331–38.
- 737 ———. 2015b. "Mutational Analysis of Measles Virus Suggests Constraints on Antigenic
738 Variation of the Glycoproteins." *Cell Reports* 11 (9): 1331–38.
- 739 Hadfield, James, Colin Megill, Sidney M. Bell, John Huddleston, Barney Potter, Charlton
740 Callender, Pavel Sagulenko, Trevor Bedford, and Richard A. Neher. 2018. "Nextstrain:
741 Real-Time Tracking of Pathogen Evolution." *Bioinformatics* 34 (23): 4121–23.
- 742 Hamre, D., and M. Beem. 1972. "Virologic Studies of Acute Respiratory Disease in Young

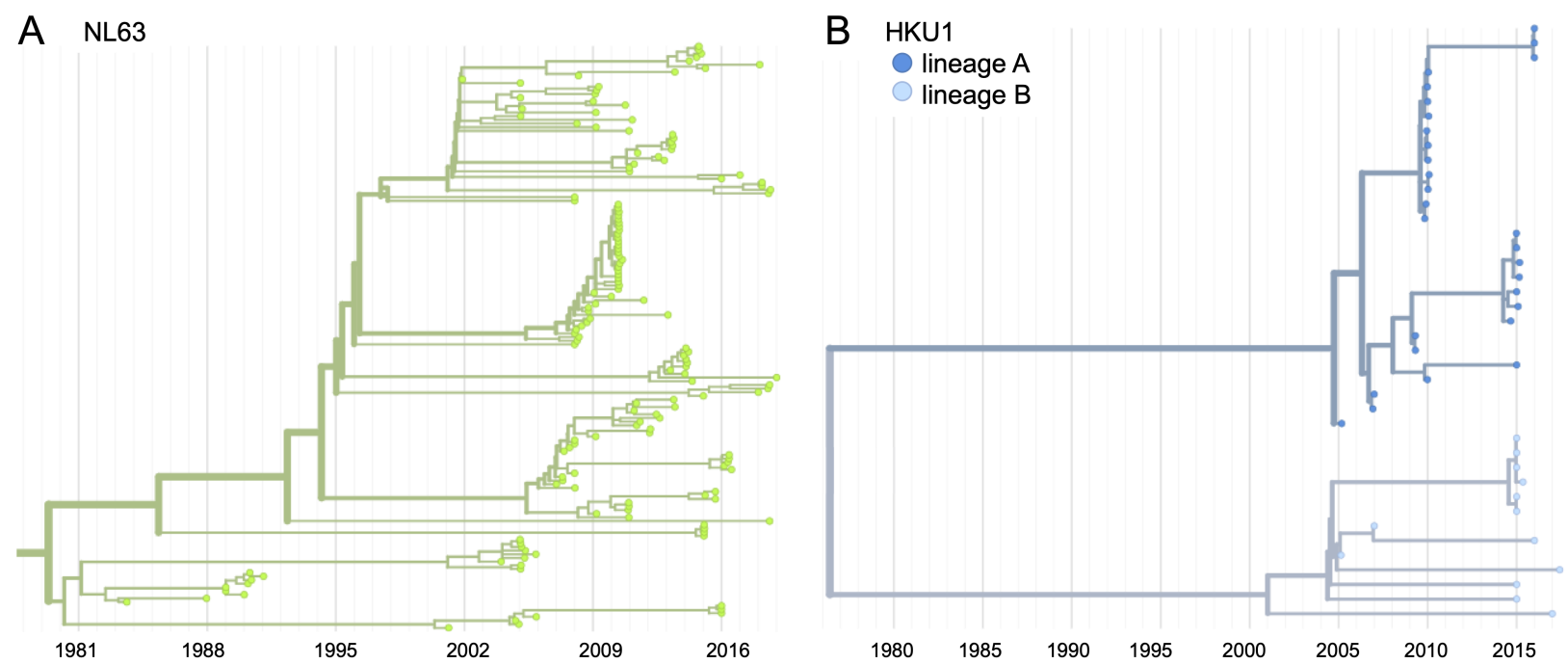
- 743 Adults. V. Coronavirus 229E Infections during Six Years of Surveillance." *American*
744 *Journal of Epidemiology* 96 (2): 94–106.
- 745 Heikkinen, Terho, and Asko Järvinen. 2003. "The Common Cold." *The Lancet* 361 (9351): 51–
746 59.
- 747 Hofmann, Heike, Graham Simmons, Andrew J. Rennekamp, Chawaree Chaipan, Thomas
748 Gramberg, Elke Heck, Martina Geier, et al. 2006. "Highly Conserved Regions within the
749 Spike Proteins of Human Coronaviruses 229E and NL63 Determine Recognition of Their
750 Respective Cellular Receptors." *Journal of Virology* 80 (17): 8639–52.
- 751 Hon, Chung-Chau, Tsan-Yuk Lam, Zheng-Li Shi, Alexei J. Drummond, Chi-Wai Yip, Fanya
752 Zeng, Pui-Yi Lam, and Frederick Chi-Ching Leung. 2008. "Evidence of the Recombinant
753 Origin of a Bat Severe Acute Respiratory Syndrome (SARS)-like Coronavirus and Its
754 Implications on the Direct Ancestor of SARS Coronavirus." *Journal of Virology* 82 (4):
755 1819–26.
- 756 Hulswit, Ruben J. G., Yifei Lang, Mark J. G. Bakkers, Wentao Li, Zeshi Li, Arie Schouten, Bram
757 Ophorst, et al. 2019. "Human Coronaviruses OC43 and HKU1 Bind to 9-O-Acetylated
758 Sialic Acids via a Conserved Receptor-Binding Site in Spike Protein Domain A."
759 *Proceedings of the National Academy of Sciences of the United States of America* 116
760 (7): 2681–90.
- 761 Jariani, Abbas, Christopher Warth, Koen Deforche, Pieter Libin, Alexei J. Drummond, Andrew
762 Rambaut, Frederick A. Matsen Iv, and Kristof Theys. 2019. "SANTA-SIM: Simulating
763 Viral Sequence Evolution Dynamics under Selection and Recombination." *Virus*
764 *Evolution* 5 (1): vez003.
- 765 Katoh, Kazutaka, Kazuharu Misawa, Kei-Ichi Kuma, and Takashi Miyata. 2002. "MAFFT: A
766 Novel Method for Rapid Multiple Sequence Alignment Based on Fast Fourier
767 Transform." *Nucleic Acids Research* 30 (14): 3059–66.
- 768 Kiyuka, Patience K., Charles N. Agoti, Patrick K. Munywoki, Regina Njeru, Anne Bett, James R.
769 Otieno, Grieven P. Otieno, et al. 2018. "Human Coronavirus NL63 Molecular
770 Epidemiology and Evolutionary Patterns in Rural Coastal Kenya." *The Journal of*
771 *Infectious Diseases* 217 (11): 1728–39.
- 772 Komabayashi, Kenichi, Yohei Matoba, Shizuka Tanaka, Junji Seto, Yoko Aoki, Tatsuya Ikeda,
773 Yoshitaka Shimotai, Yoko Matsuzaki, Tsutomu Itagaki, and Katsumi Mizuta. 2020.
774 "Longitudinal Epidemiology of Human Coronavirus OC43 in Yamagata, Japan, 2010–
775 2017: Two Groups Based on Spike Gene Appear One after Another." *Journal of Medical*
776 *Virology* 7 (August): 825.
- 777 Kosakovsky Pond, Sergei L., David Posada, Michael B. Gravenor, Christopher H. Woelk, and
778 Simon D. W. Frost. 2006. "Automated Phylogenetic Detection of Recombination Using a
779 Genetic Algorithm." *Molecular Biology and Evolution* 23 (10): 1891–1901.
- 780 Köster, Johannes, and Sven Rahmann. 2012. "Snakemake—a Scalable Bioinformatics
781 Workflow Engine." *Bioinformatics* 28 (19): 2520–22.
- 782 Krammer, Florian. 2020. "SARS-CoV-2 Vaccines in Development." *Nature*, September.
783 <https://doi.org/10.1038/s41586-020-2798-3>.
- 784 Kucharski, Adam J., Justin Lessler, Jonathan M. Read, Huachen Zhu, Chao Qiang Jiang, Yi
785 Guan, Derek A. T. Cummings, and Steven Riley. 2015. "Estimating the Life Course of
786 Influenza A(H3N2) Antibody Responses from Cross-Sectional Data." *PLOS Biology*.
787 <https://doi.org/10.1371/journal.pbio.1002082>.
- 788 Lau, Susanna K. P., Paul Lee, Alan K. L. Tsang, Cyril C. Y. Yip, Herman Tse, Rodney A. Lee,
789 Lok-Yee So, et al. 2011. "Molecular Epidemiology of Human Coronavirus OC43 Reveals
790 Evolution of Different Genotypes over Time and Recent Emergence of a Novel
791 Genotype Due to Natural Recombination." *Journal of Virology* 85 (21): 11325–37.
- 792 Li, Fang. 2016. "Structure, Function, and Evolution of Coronavirus Spike Proteins." *Annual*
793 *Review of Virology* 3 (1): 237–61.

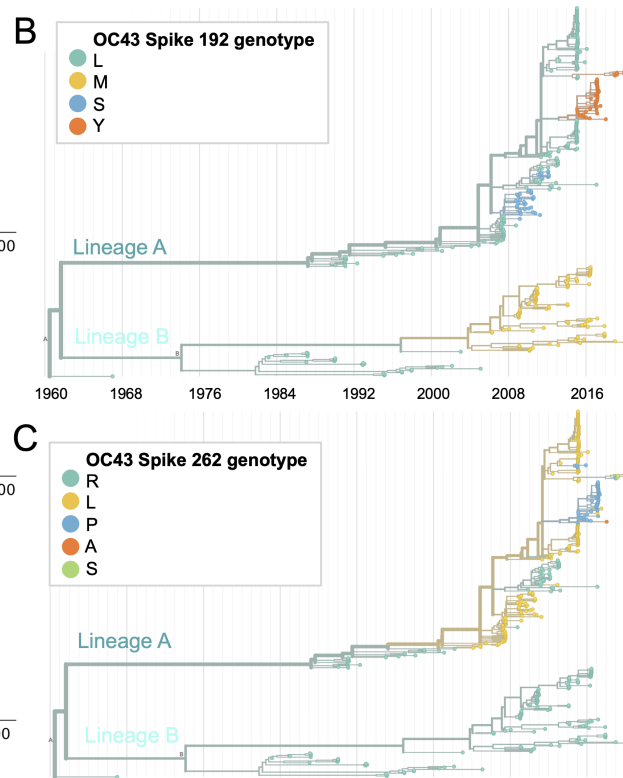
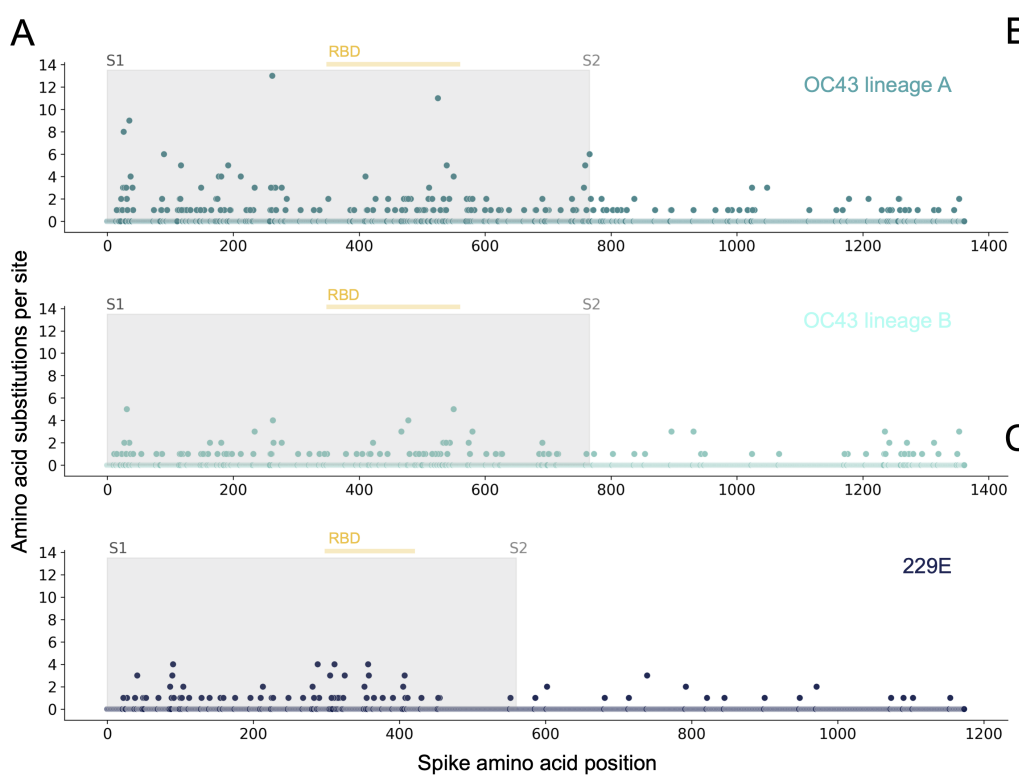
- 794 Li, Zhijie, Aidan Ca Tomlinson, Alan Hm Wong, Dongxia Zhou, Marc Desforges, Pierre J.
795 Talbot, Samir Benlekbir, John L. Rubinstein, and James M. Rini. 2019. "The Human
796 Coronavirus HCoV-229E S-Protein Structure and Receptor Binding." *eLife* 8 (October).
797 <https://doi.org/10.7554/eLife.51230>.
- 798 Liu, Ding X., Jia Q. Liang, and To S. Fung. 2020. "Human Coronavirus-229E, -OC43, -NL63,
799 and -HKU1." *Reference Module in Life Sciences*. <https://doi.org/10.1016/b978-0-12-809633-8.21501-x>.
- 800 Liu, Lihong, Pengfei Wang, Manoj S. Nair, Jian Yu, Micah Rapp, Qian Wang, Yang Luo, et al.
801 2020. "Potent Neutralizing Antibodies against Multiple Epitopes on SARS-CoV-2 Spike."
802 *Nature* 584 (7821): 450–56.
- 803 Luksza, Marta, and Michael Lässig. 2014. "A Predictive Fitness Model for Influenza." *Nature* 507
804 (7490): 57–61.
- 805 McIntosh, Kenneth. 1974. "Coronaviruses: A Comparative Review." In *Current Topics in
806 Microbiology and Immunology / Ergebnisse Der Mikrobiologie Und Immunitätsforschung*,
807 85–129. Springer Berlin Heidelberg.
- 808 Monto, Arnold S., and Sook K. Lim. 1974. "The Tecumseh Study of Respiratory Illness. VI.
809 Frequency of and Relationship between Outbreaks of Coronavims Infection." *The
810 Journal of Infectious Diseases* 129 (3): 271–76.
- 811 Murrell, Ben, Joel O. Wertheim, Sasha Moola, Thomas Weighill, Konrad Scheffler, and Sergei L.
812 Kosakovsky Pond. 2012. "Detecting Individual Sites Subject to Episodic Diversifying
813 Selection." *PLoS Genetics* 8 (7): e1002764.
- 814 Nguyen, Lam-Tung, Heiko A. Schmidt, Arndt von Haeseler, and Bui Quang Minh. 2015. "IQ-
815 TREE: A Fast and Effective Stochastic Algorithm for Estimating Maximum-Likelihood
816 Phylogenies." *Molecular Biology and Evolution* 32 (1): 268–74.
- 817 Pasternak, Alexander O., Willy J. M. Spaan, and Eric J. Snijder. 2006. "Nidovirus Transcription:
818 How to Make Sense...?" *The Journal of General Virology* 87 (6): 1403–21.
- 819 Pickett, Brett E., Eva L. Sadat, Yun Zhang, Jyothi M. Noronha, R. Burke Squires, Victoria Hunt,
820 Mengya Liu, et al. 2012. "ViPR: An Open Bioinformatics Database and Analysis
821 Resource for Virology Research." *Nucleic Acids Research* 40 (Database issue): D593-8.
- 822 Rambaut, Andrew, Oliver G. Pybus, Martha I. Nelson, Cecile Viboud, Jeffery K. Taubenberger,
823 and Edward C. Holmes. 2008. "The Genomic and Epidemiological Dynamics of Human
824 Influenza A Virus." *Nature* 453 (7195): 615–19.
- 825 Reed, Sylvia E. 1984. "The Behaviour of Recent Isolates of Human Respiratory Coronavirus in
826 Vitro and in Volunteers: Evidence of Heterogeneity among 229E-Related Strains."
827 *Journal of Medical Virology* 13 (2): 179–92.
- 828 Ren, Lili, Yue Zhang, Jianguo Li, Yan Xiao, Jing Zhang, Ying Wang, Lan Chen, Gláucia
829 Paranhos-Baccalà, and Jianwei Wang. 2015. "Genetic Drift of Human Coronavirus
830 OC43 Spike Gene during Adaptive Evolution." *Scientific Reports* 5 (June): 11451.
- 831 Sagulenko, Pavel, Vadim Puller, and Richard A. Neher. 2018. "TreeTime: Maximum-Likelihood
832 Phylogenetic Analysis." *Virus Evolution* 4 (1): vex042.
- 833 Smith, Derek J., Alan S. Lapedes, Jan C. de Jong, Theo M. Bestebroer, Guus F. Rimmelzwaan,
834 Albert D. M. E. Osterhaus, and Ron A. M. Fouchier. 2004. "Mapping the Antigenic and
835 Genetic Evolution of Influenza Virus." *Science* 305 (5682): 371–76.
- 836 Vijgen, Leen, Philippe Lemey, Els Keyaerts, and Marc Van Ranst. 2005. "Genetic Variability of
837 Human Respiratory Coronavirus OC43." *Journal of Virology*.
- 838 Volz, Erik M., Katia Koelle, and Trevor Bedford. 2013. "Viral Phylodynamics." *PLoS
839 Computational Biology* 9 (3): e1002947.
- 840 Weaver, Steven, Stephen D. Shank, Stephanie J. Spielman, Michael Li, Spencer V. Muse, and
841 Sergei L. Kosakovsky Pond. 2018. "Datamonkey 2.0: A Modern Web Application for
842 Characterizing Selective and Other Evolutionary Processes." *Molecular Biology and
843 Evolution*. <https://doi.org/10.1093/molbev/msx335>.

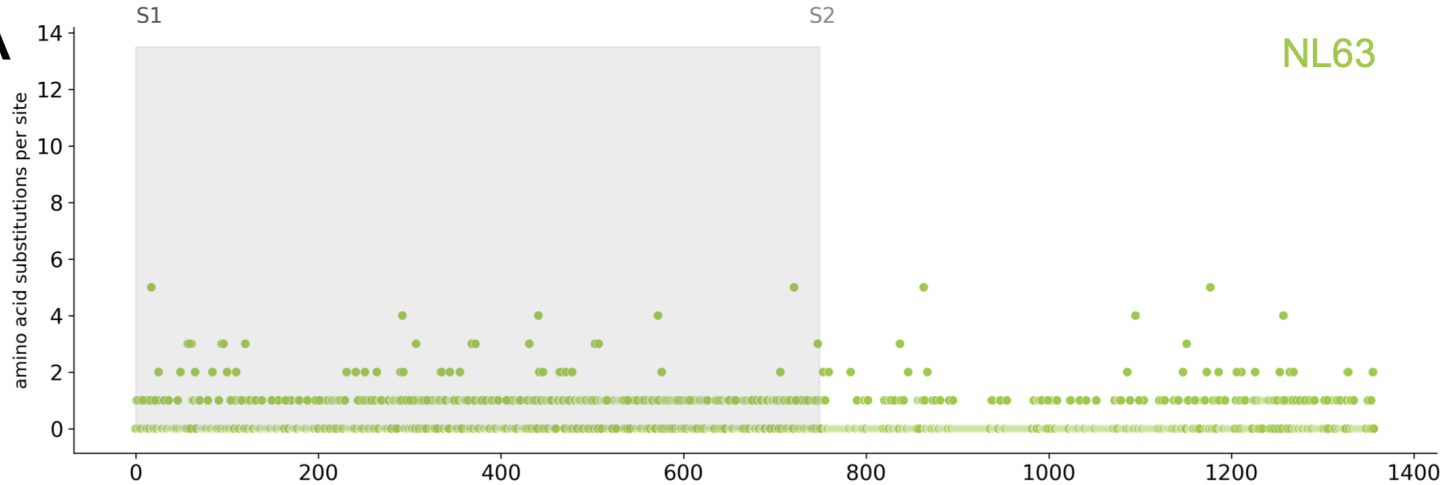
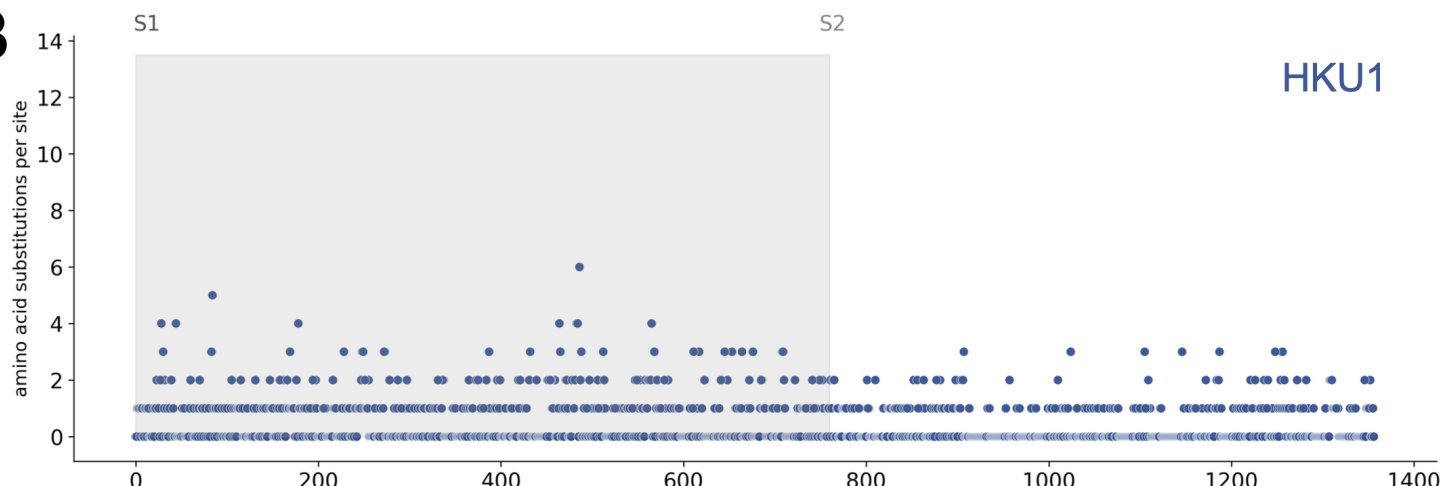
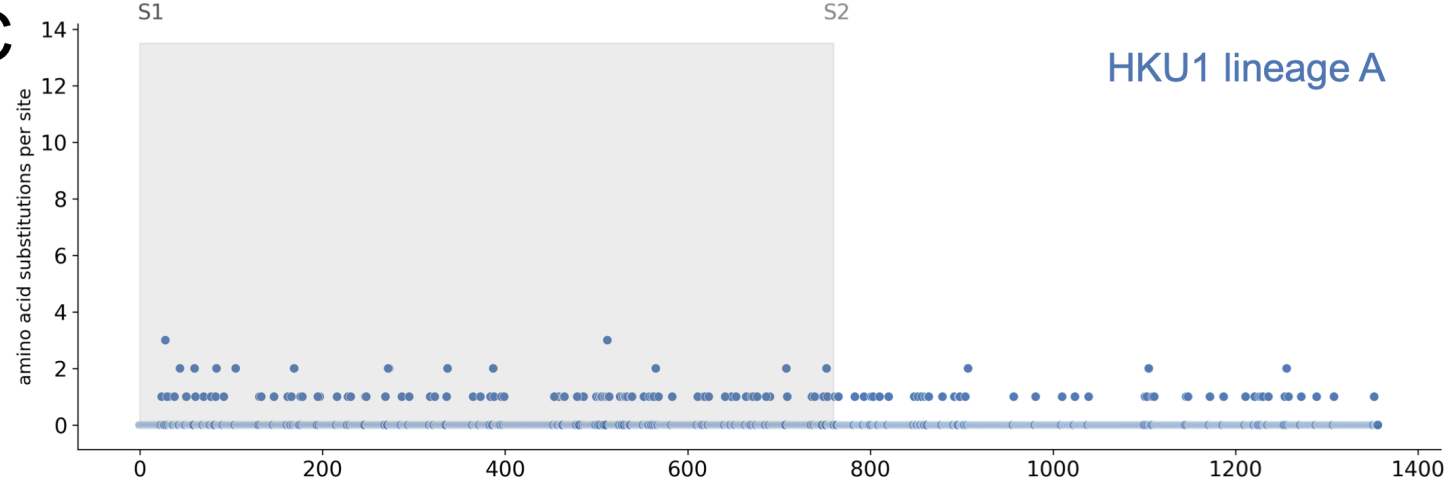
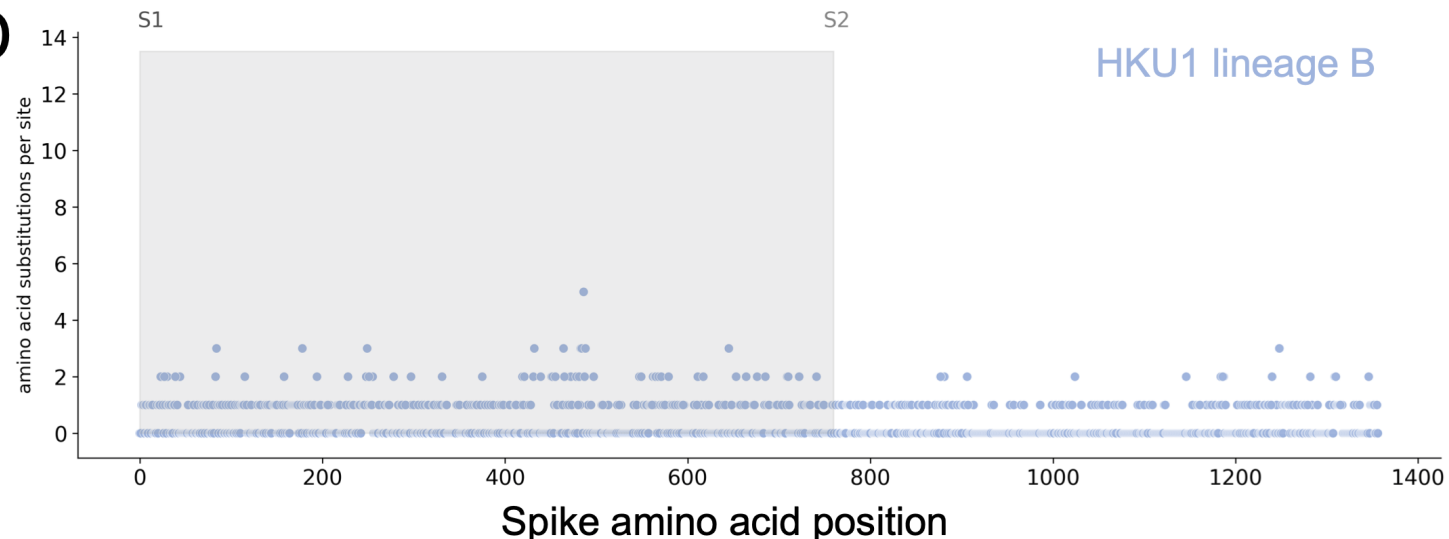
- 845 Woo, Patrick C. Y., Susanna K. P. Lau, Yi Huang, and Kwok-Yung Yuen. 2009. "Coronavirus
846 Diversity, Phylogeny and Interspecies Jumping." *Experimental Biology and Medicine*
847 234 (10): 1117–27.
- 848 Yang, Z. 2000. "Maximum Likelihood Estimation on Large Phylogenies and Analysis of Adaptive
849 Evolution in Human Influenza Virus A." *Journal of Molecular Evolution* 51 (5): 423–32.
- 850 Zanini, Fabio, Johanna Brodin, Lina Thebo, Christa Lanz, Göran Bratt, Jan Albert, and Richard
851 A. Neher. 2015. "Population Genomics of Intrapatient HIV-1 Evolution." *eLife* 4
852 (December). <https://doi.org/10.7554/eLife.11282>.
- 853 Zhang, Senyan, Panpan Zhou, Pengfei Wang, Yangyang Li, Liwei Jiang, Wenxu Jia, Han
854 Wang, et al. 2018. "Structural Definition of a Unique Neutralization Epitope on the
855 Receptor-Binding Domain of MERS-CoV Spike Glycoprotein." *Cell Reports*.
856 <https://doi.org/10.1016/j.celrep.2018.06.041>.
- 857 Zhang, Yue, Jianguo Li, Yan Xiao, Jing Zhang, Ying Wang, Lan Chen, Gláucia Paranhos-
858 Baccalà, Lili Ren, and Jianwei Wang. 2015. "Genotype Shift in Human Coronavirus
859 OC43 and Emergence of a Novel Genotype by Natural Recombination." *Journal of
860 Infection*. <https://doi.org/10.1016/j.jinf.2014.12.005>.
- 861 Zhou, Haixia, Yingzhu Chen, Shuyuan Zhang, Peihua Niu, Kun Qin, Wenxu Jia, Baoying
862 Huang, et al. 2019. "Structural Definition of a Neutralization Epitope on the N-Terminal
863 Domain of MERS-CoV Spike Glycoprotein." *Nature Communications*.
864 <https://doi.org/10.1038/s41467-019-10897-4>.
- 865 Zhu, Yun, Changchong Li, Li Chen, Baoping Xu, Yunlian Zhou, Ling Cao, Yunxiao Shang, et al.
866 2018. "A Novel Human Coronavirus OC43 Genotype Detected in Mainland China."
867 *Emerging Microbes & Infections* 7 (1): 173.

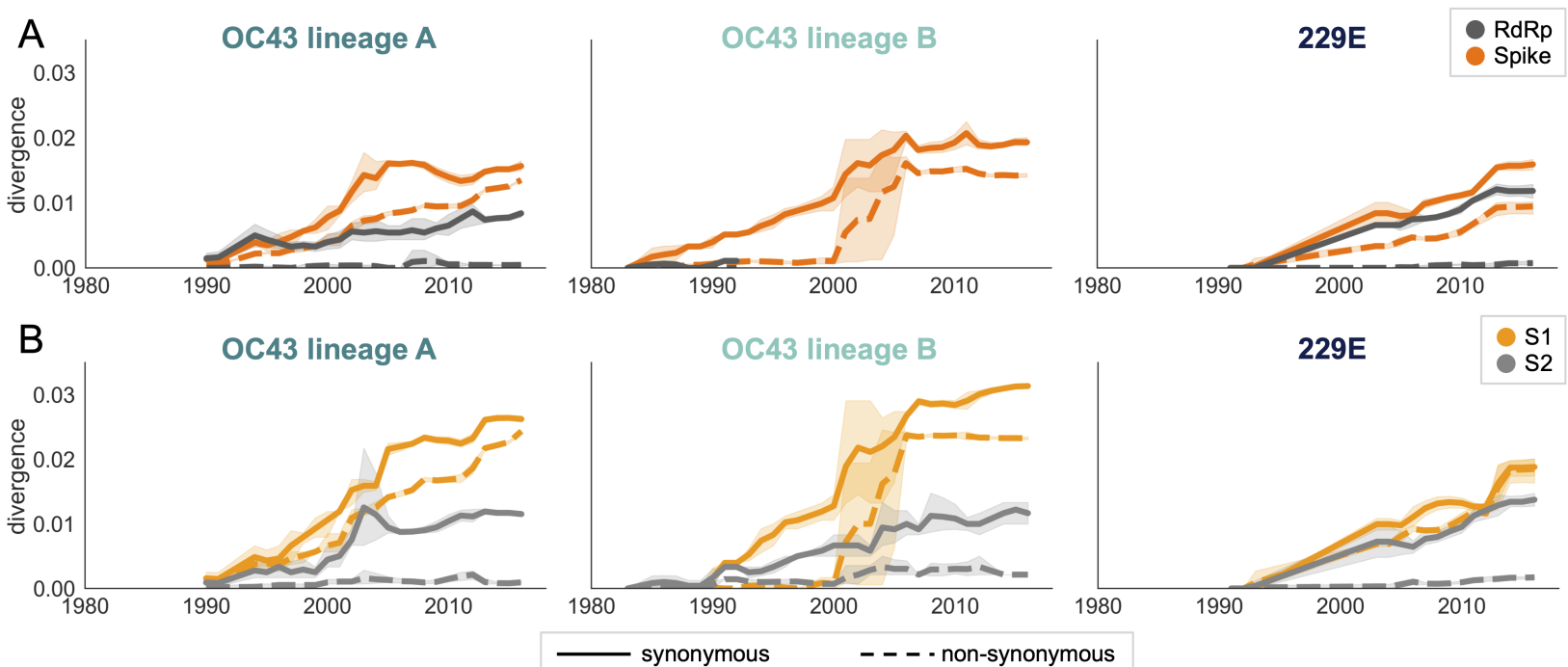


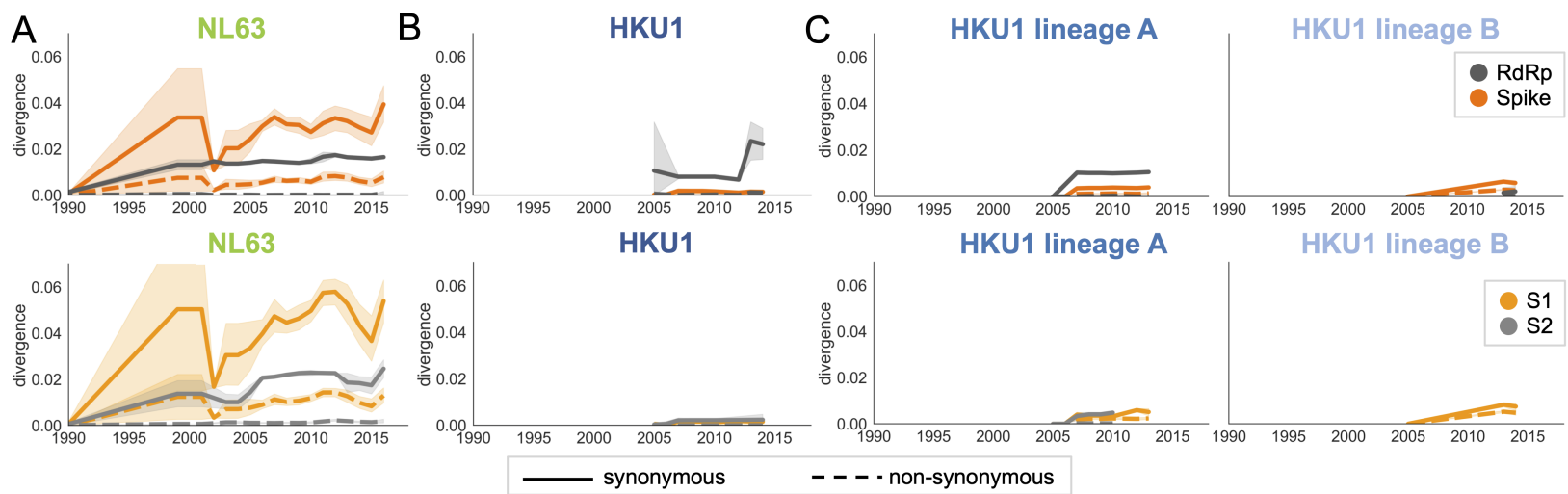


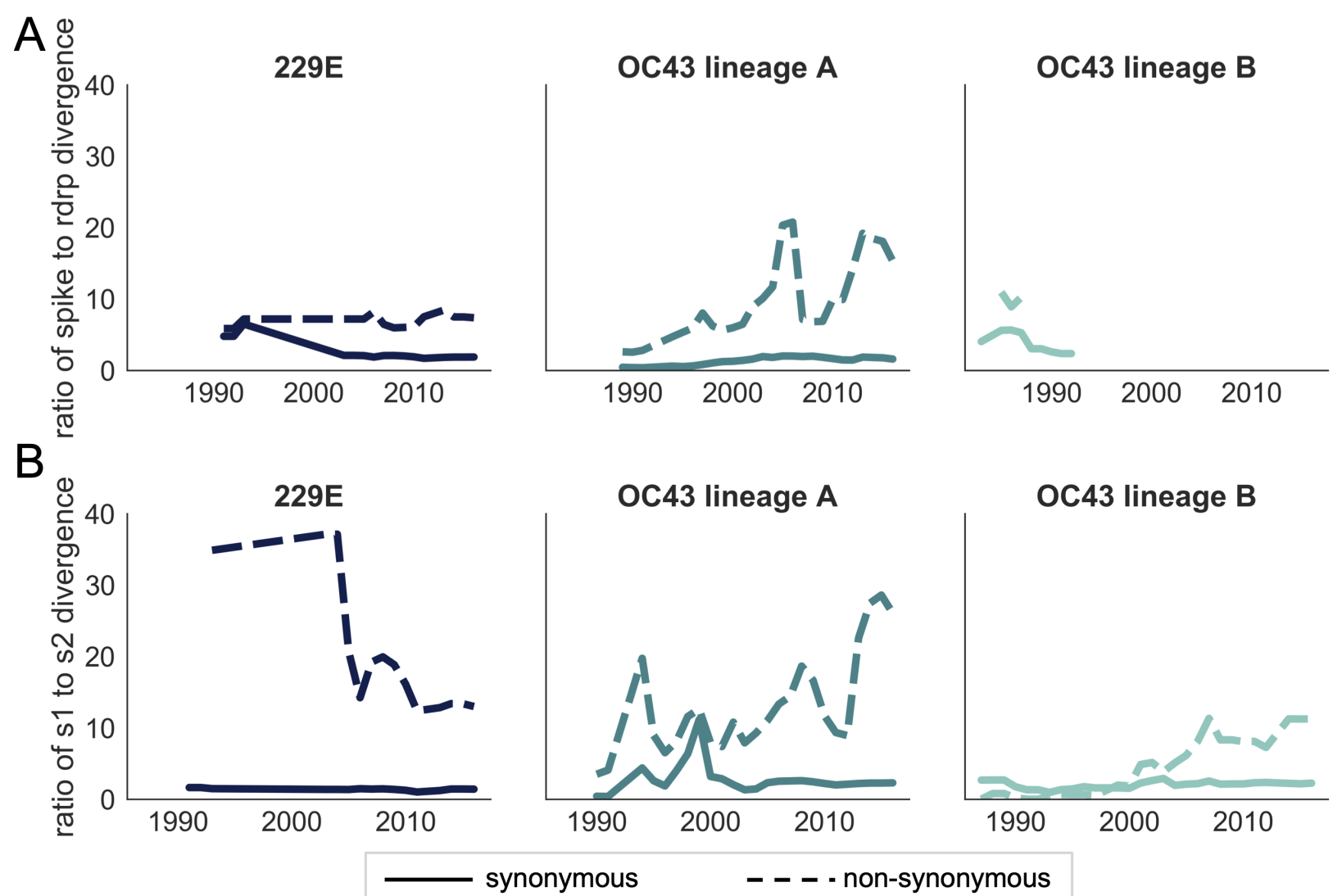


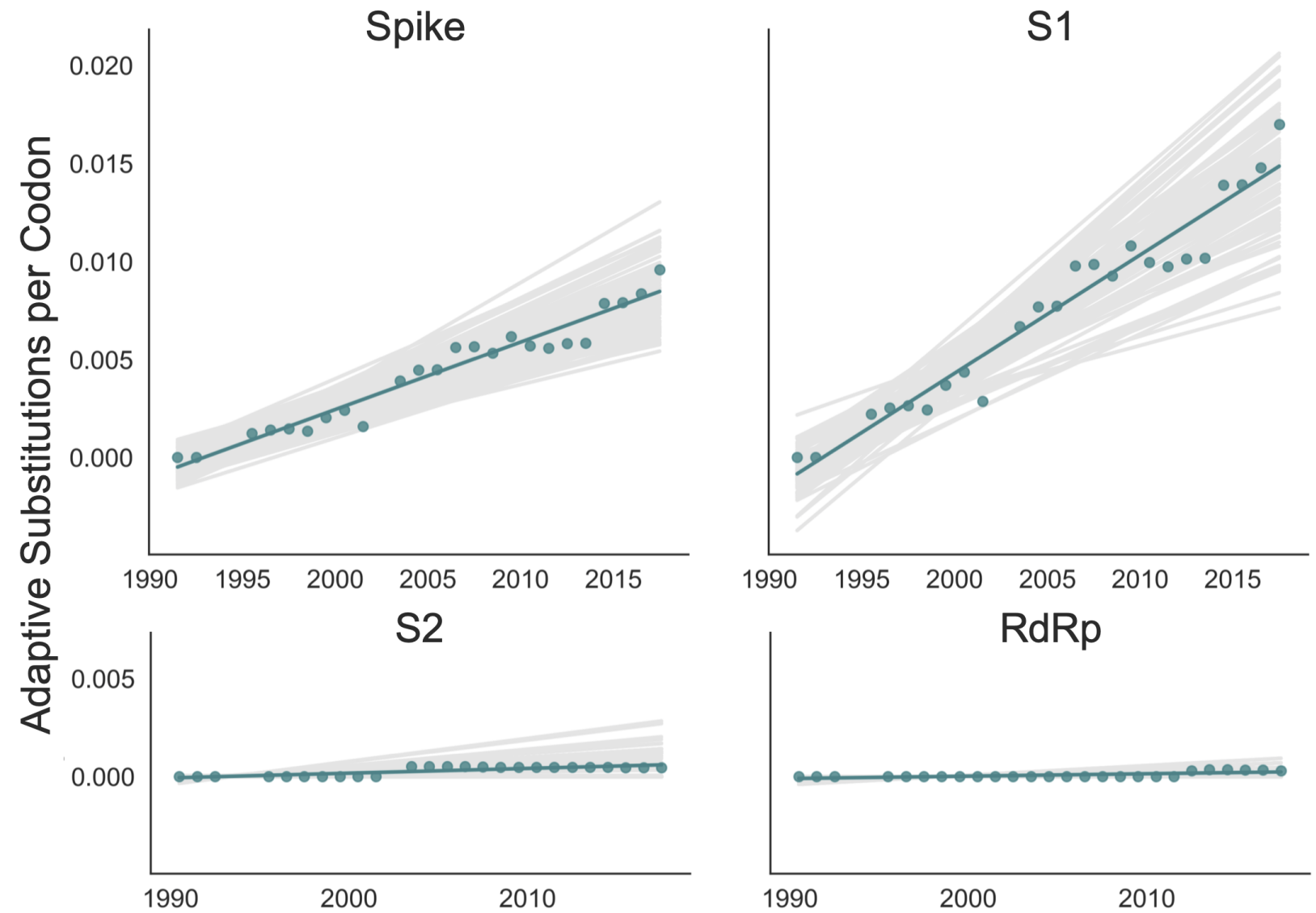


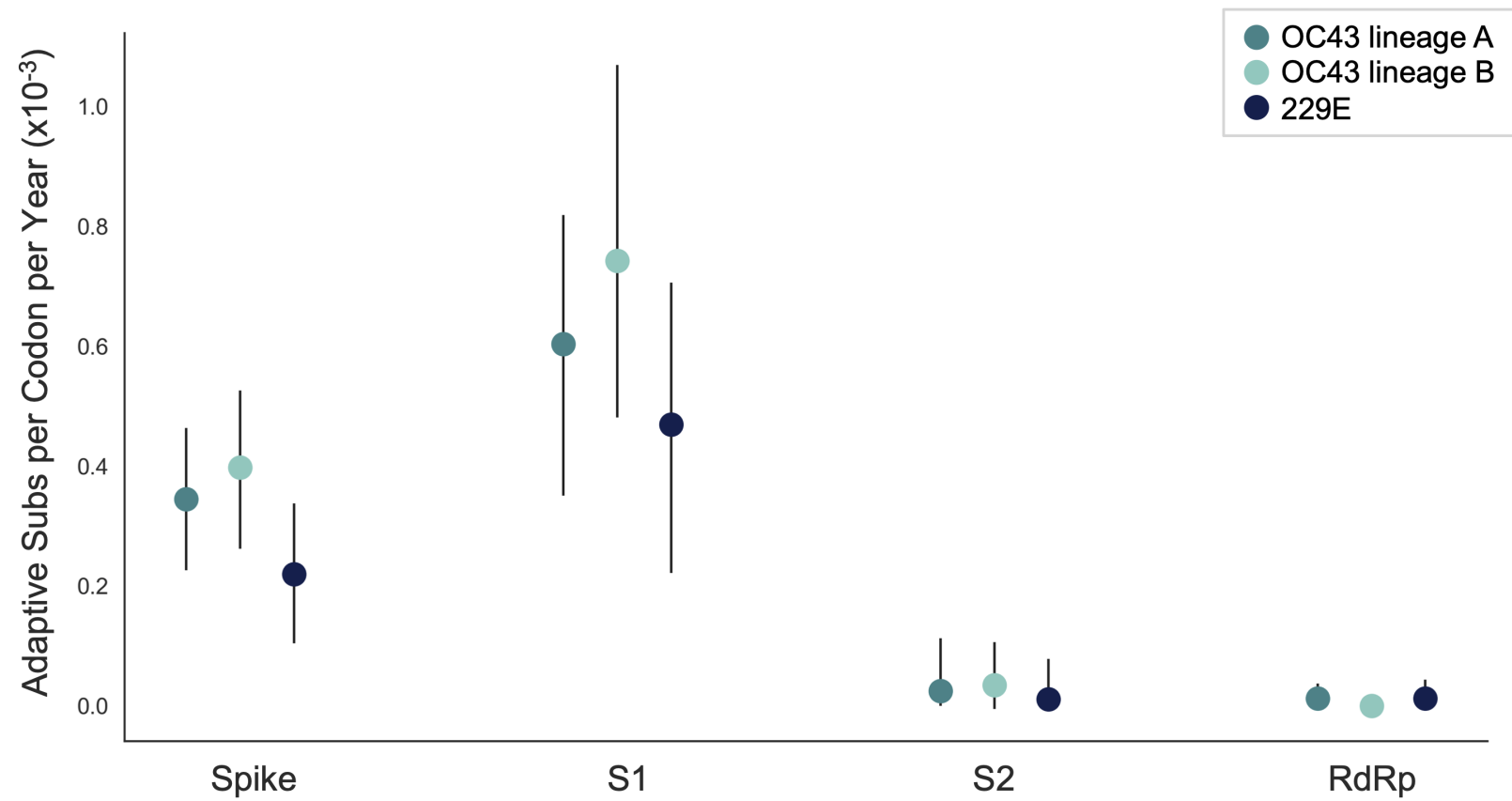
A**B****C****D**

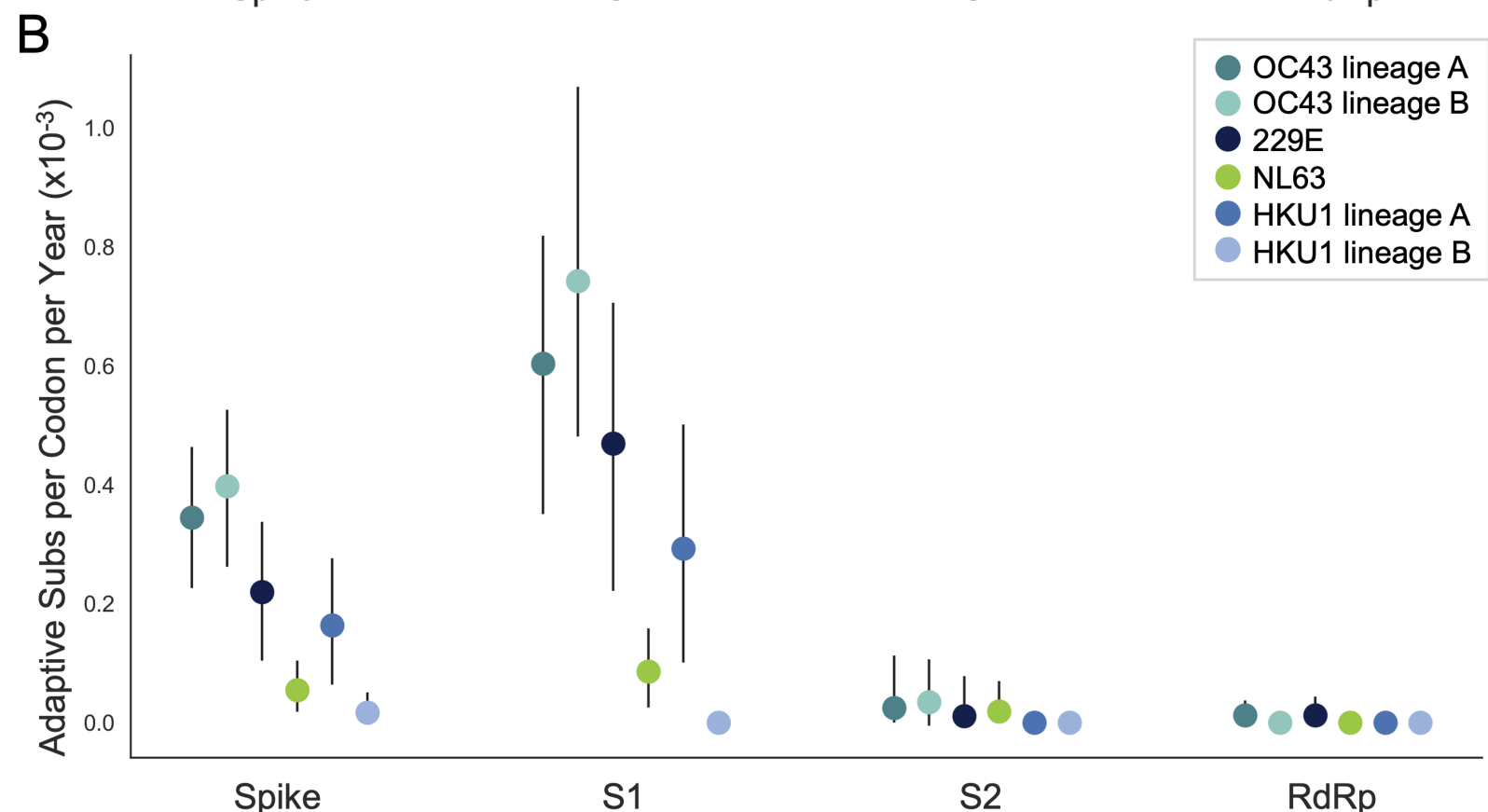
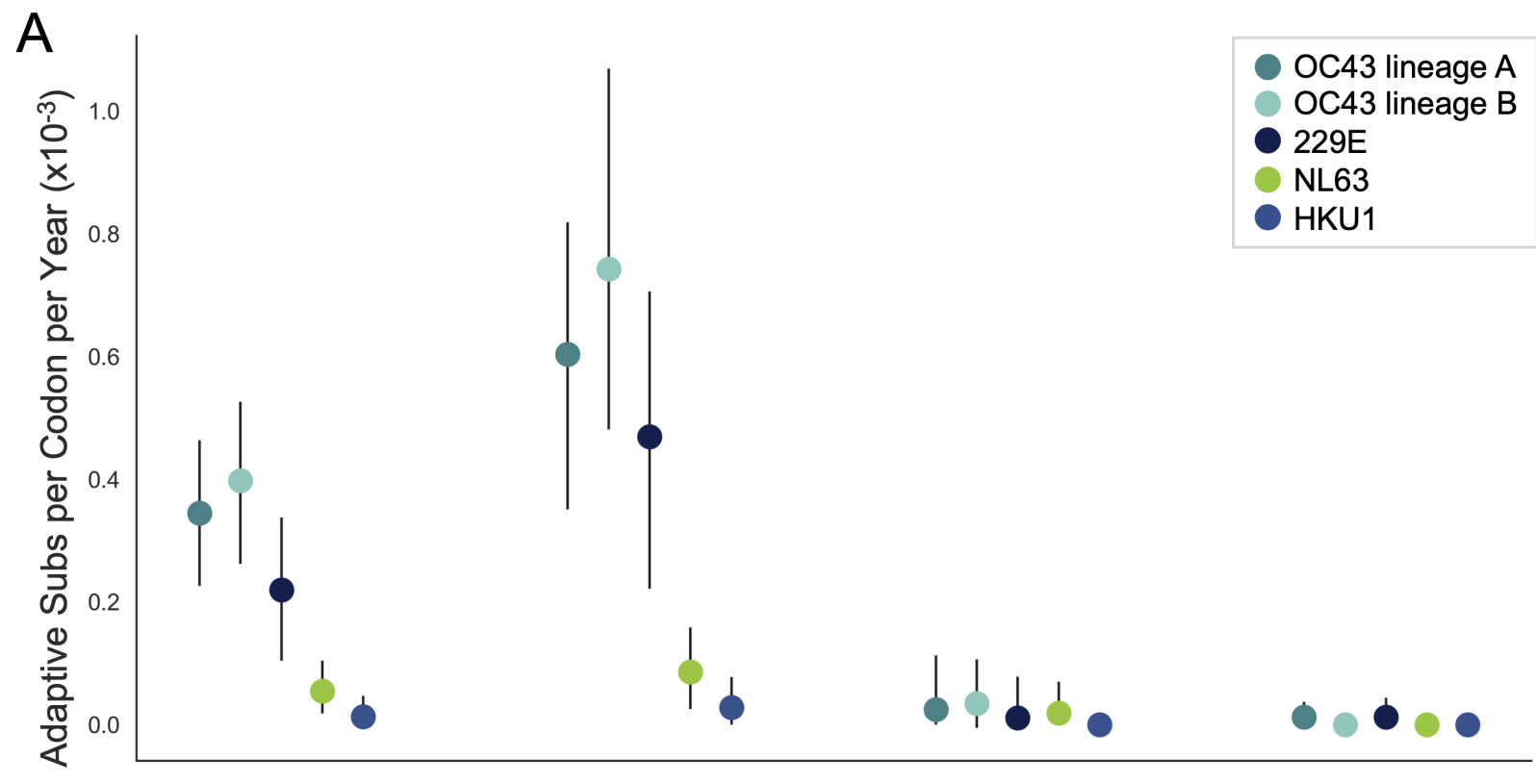


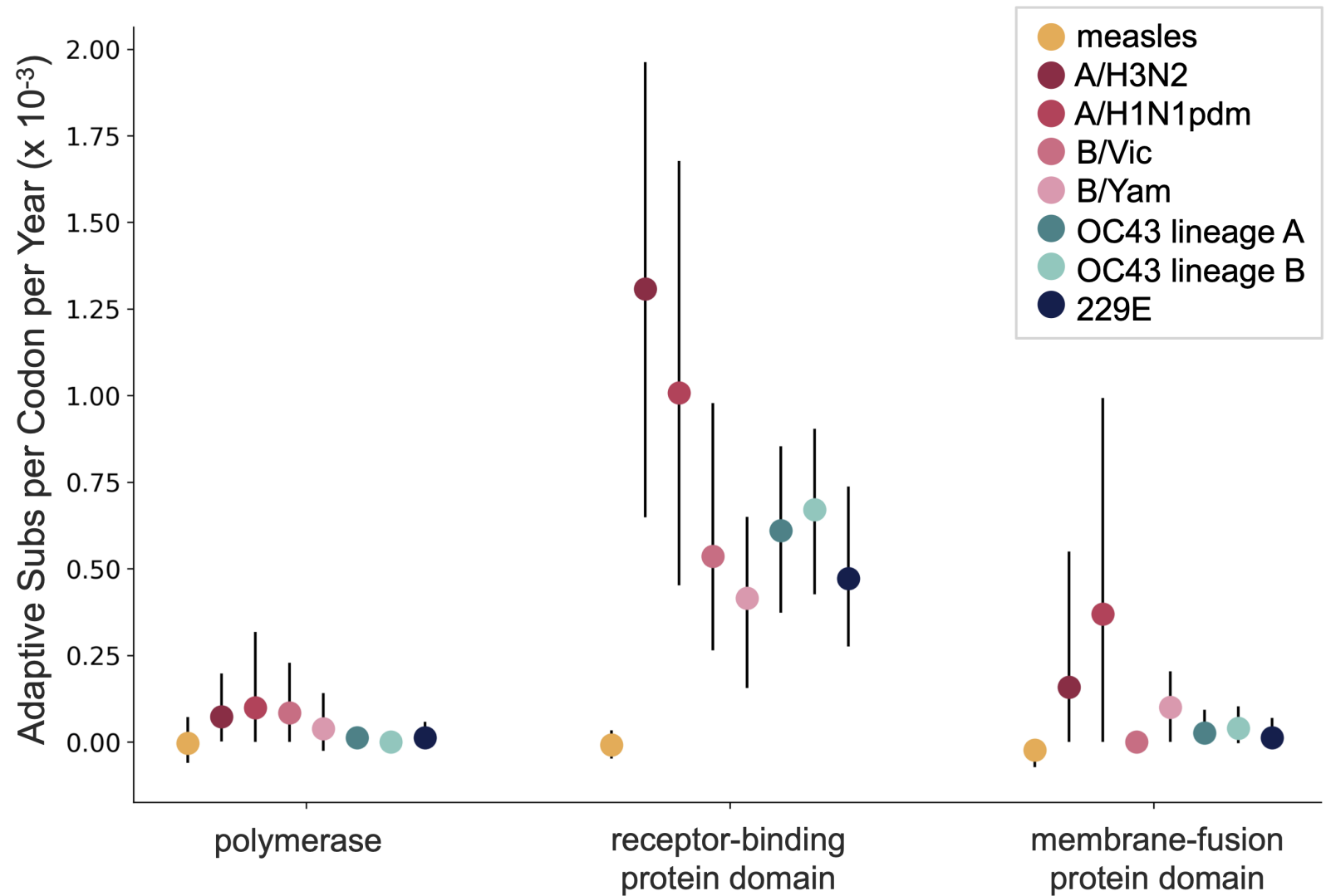


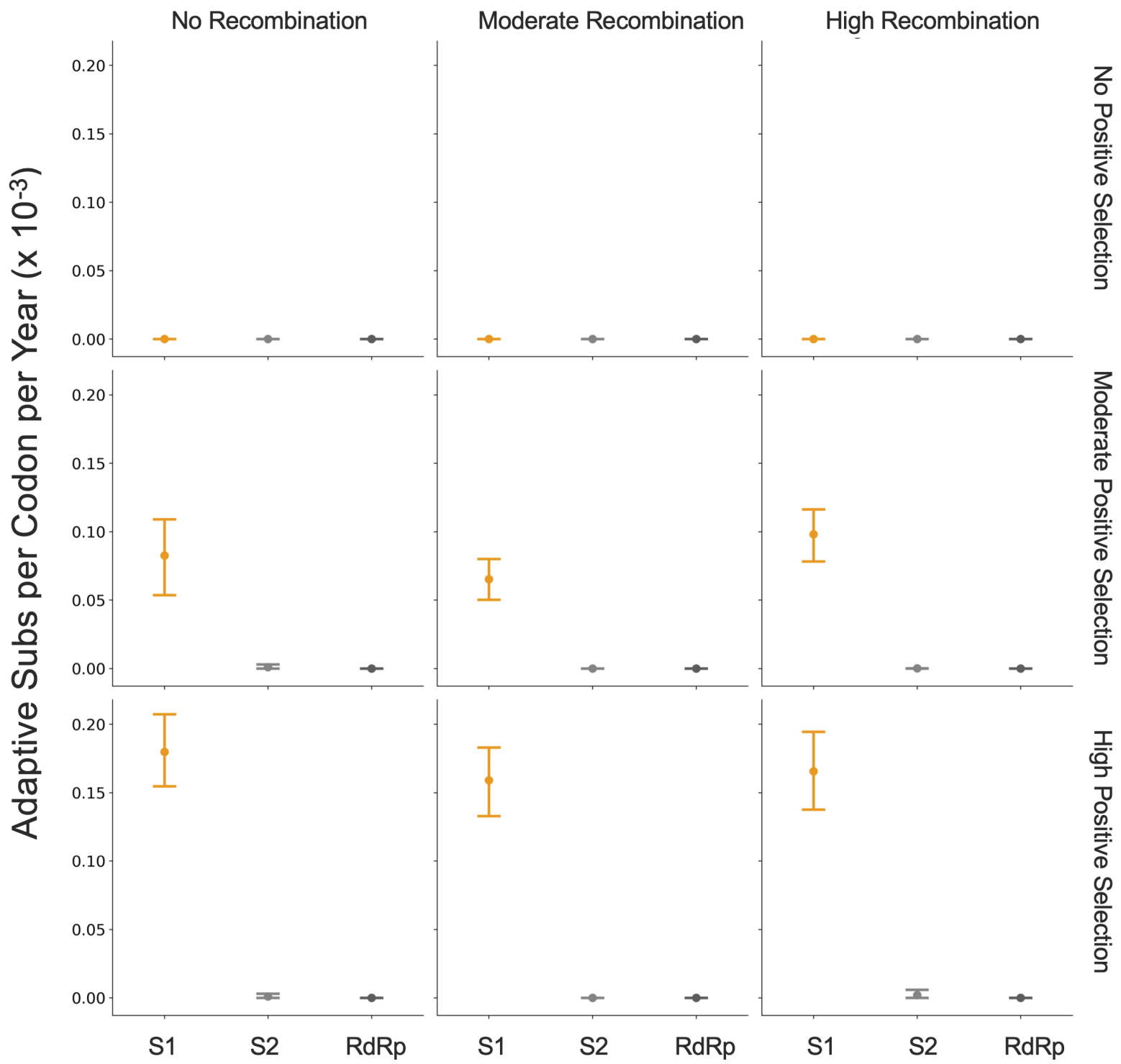


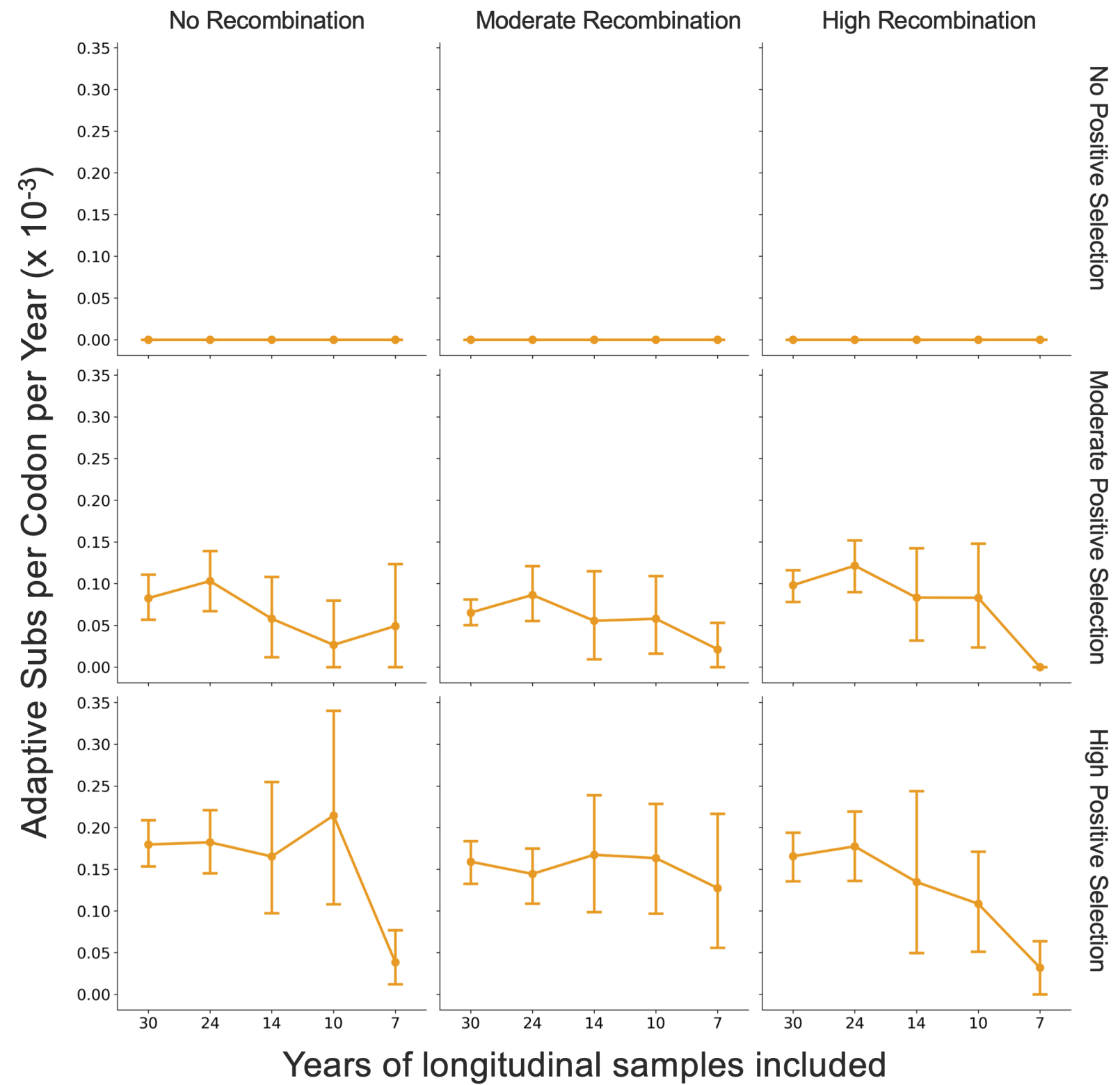




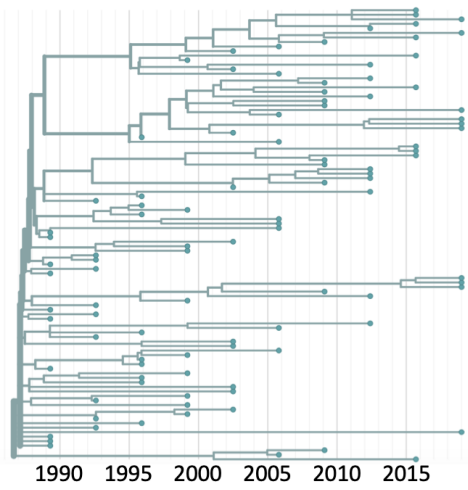




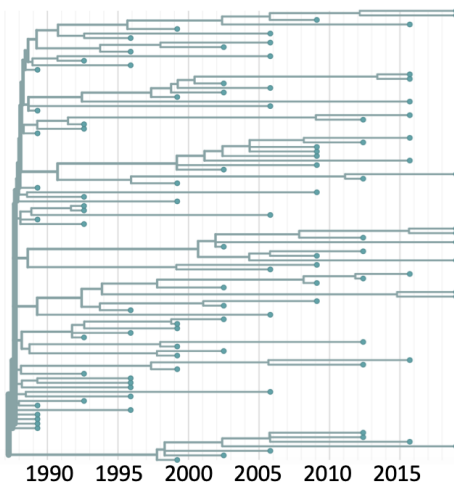




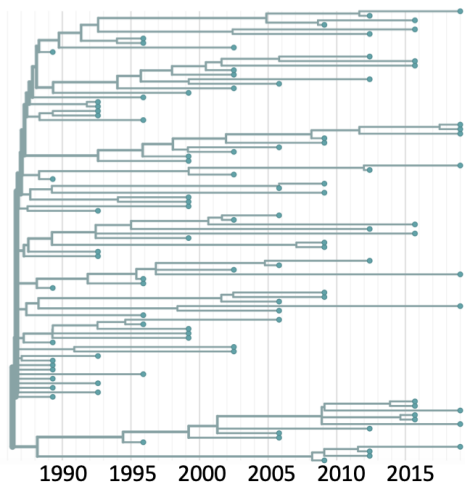
No Recombination



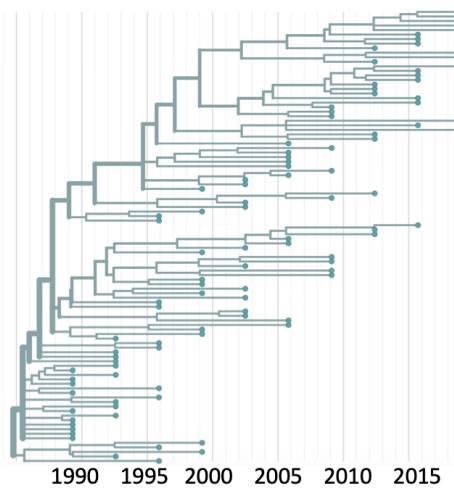
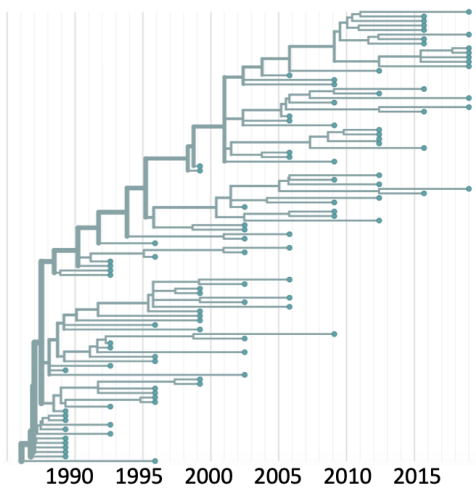
Moderate Recombination



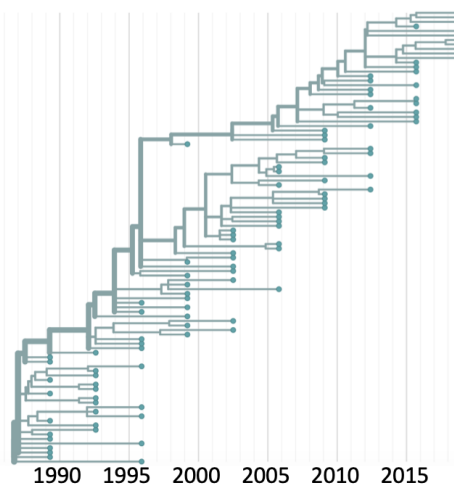
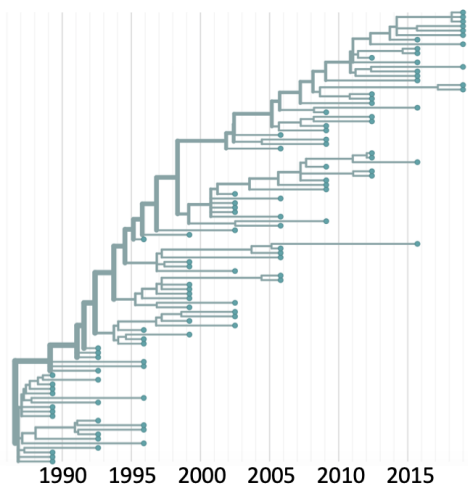
High Recombination



No Positive Selection



Moderate Positive Selection



High Positive Selection